Metrology-Based Techniques for Optical System Alignment for the OSIRIS-Rx Visual and InfraRed Spectrometer

by

Jerrod Young

A Report Submitted to the Faculty of the

DEPARTMENT OF OPTICAL SCIENCES

In Partial Fulfillment of the Requirements

For the Degree of

MASTER OF SCIENCE

In the Graduate College

THE UNIVERSITY OF ARIZONA

2018

TABLE OF CONTENTS

Chapter Page

1.0 Introduction 1

1.1 Brief Overview of Metrology Instrumentation 1

1.2 Introduction to uncertainty 3

2.0 Metrology instrumentation and Measurement techniques 4

2.1 Laser tracker 4

2.1.1 Measurement Modes 5

2.1.2 Tracking 6

2.2 Laser radar 7

2.2.1 Type of measurements 8

2.3 measurement routines: Laser Tracker/Rader Operation 12

2.3.1 Measuring Through Fold Mirror 12

2.3.2 Direct and Through 13

2.4 Spatial Analyzer™ 14

2.4.1 Best Fit Transformation 14

2.5 Theodolites 17

2.5.1 Data Analysis 23

2.6 Laser Radar, Laser Tracker, and Theodolites tied into Common Coordinate System 31

3.0 The OSIRIS-Rex Infra-red Spectrometer (OVIRS) 34

3.1 Alignment Philosophy 35

3.2 Flight Mirror Characterization 37

3.3 Flight Mirror Mounting Assembly 41

3.4 Optical bench characterization and coordinate system definition 46

3.5 Field stop Calibration 48

3.5.1 Surrogate Field Stop 48

3.5.2 Flight Field Stop 49

3.6 Mirror Installation 51

3.6.1 Primary Mirror 51

3.6.2 Secondary Mirror 52

3.7 Vignetting (FOV) Test 54

3.8 Detector 55

3.8.1 Detector Mask and Housing 55

3.8.2 Beam Characterization 56

3.8.3 Nominal Location 58

3.9 Theodolite System Throughput Test 60

3.10 System Measurement 62

3.10.1 Pre-Detector Installation 62

3.10.2 Post Detector Installation 65

4.0 References 70

LIST OF FIGURES

Figure Page

Figure 1-1. Micro-Vu in the cleanroom. .....

Figure 2-1. Spherically Mounted Retroreflector..... 5

Figure 2-2. Laser radar point measurement of a tooling ball. 9

Figure 2-3. Laser radar vision scan box. .....

Figure 2-4. Laser radar fast metrology scan box. .....

Figure 2-5. Laser radar metrology scan box. .....

Figure 2-6. Laser radar hole center point measurement routine. .....

Figure 2-7. Laser tracker measuring a point through a fold mirror. 12

Figure 2-8. Laser tracker "Direct and Through" measurement routine. 13

Figure 2-9. Laser Radar survey of the James Webb Space Telescope's Optical Telescope Element 16

Figure 2-10. Auto-collimation of theodolites [8]..... 18

Figure 2-11. Optical cube face convention [8]. .....

Figure 2-12. Schematic showing OAFDAM coordinate system definition and angle nomenclature [8]. 19

Figure 2-13. Theodolite elevation-zenith relationship [7]. .....

Figure 2-14. Primary theodolite as fixed azimuth reference [8]. 22

Figure 2-15. Calculating roll values [11]. 23

Figure 2-16. Vector translation to origin [8]..... 24

Figure 2-17. Coordinate system rotation [8]. 25

Figure 2-18. Vector normalization [8]. 25

Figure 2-19. Direction cosines [11]. 26

Figure 2-20. Generic metrology schematic..... 31

Figure 3-1. Ray trace of OVIRS optical system. .....

Figure 3-2. Process flow for OVIRS alignment plan. .....

Figure 3-3. Primary and secondary mirror schematic of alignment fiducials..... 37

Figure 3-4. Primary mirror mounted on kinematic tip/tilt stage. 38
Figure 3-5. Schematic of mirror focus characterization. .....
Figure 3-6. Surface figure map and RMS of the primary mirror in Metropro software. 39
Figure 3-7. Surface figure map and RMS of the primary mirror in Metropro software. 40
Figure 3-8. CAD model of primary mirror mounting assembly. 41
Figure 3-9. Kinematic opto-mechanical mount for mirror characterization and alignment. 42
Figure 3-10. Iterations of the interface ring for the primary mirror mount. 43
Figure 3-11. Final solid mount design for the primary mirror. .....
Figure 3-12. Obox and alignment fiducials. 46
Figure 3-13. Test configuration for the Obox. 47
Figure 3-14. Schematic of the field stop in the Obox. .....
Figure 3-15. Surrogate field stop. 49
Figure 3-16. Spatial Analyzer analysis of laser radar metrology on the field stop. 50
Figure 3-17. Primary mirror installation test setup. 51
Figure 3-18. Secondary mirror installation schematic. 53
Figure 3-19. System wavefront surface map from Metropro software. 53
Figure 3-20. Micro-Vu measurement of the detector displayed graphically in SA™. 55
Figure 3-21. Detector characterization transformed the Obox frame displayed graphically in SA™. 56
Figure 3-22. Illustration of the collimated beam in SA™. .....
Figure 3-23. SA™ depiction of the detector position with respect to the collimated beam. 58
Figure 3-24. Interferometer return from LVF. 59
Figure 3-25. Test setup for the theodolite system throughput test. 60
Figure 3-26. LVF through the theodolite recital at infinite (left) and finite (right) focus. .....
Figure 3-27. End-to-end system wavefront test schematic. 62
Figure 3-28. System wavefront error pre-vibration test results. 63
Figure 3-29. System wavefront error post-vibration test results 63
Figure 3-30. OVIRS on the vibration test plate. 66

Figure 3-31. Trending data from the interferometer and theodolite alignment test (infinite conjugate). 67

Figure 3-32. Trending data from the interferometer and theodolite alignment test (finite conjugate). 68

LIST OF TABLES

Table Page

Table 2-1. Metrology Tools 8

Table 3-1. Vignetting test results. 54

Table 3-2. Pre-Post Vibration Theodolite Test (OC1, OC2, Interferometer, Flat Mirror) 64

Table 3-3. Pre-Post Vibration Theodolite Test (OC1 and Mirrors) 64

Table 3-4. Pre-Post Vibration Laser Radar Results 65

1.0 INTRODUCTION

The Optics Branch at the National Aeronautics and Space Administration (NASA) Goddard Space Flight Center (GSFC) specialize in optical engineering and development of space-qualified optical instrumentation [1]. The Branch expertise cover the electromagnetic spectrum from x-ray astronomical spectrometers to far-infrared earth satellites. Project and missions may span from very large telescopes to subsystems and components. The Branch has five groups of specialties that allows it to participate in all phases of the instrument and optical technology development. The Branch feature an optical design group, wavefront sensing group, component group, fabrication group, and an alignment, integration, and test group. This paper will focus on techniques and activities of the optical Alignment, Integration, and Test (AI&T) group.

The AI&T group specializes in optical and opto-mechanical alignment and metrology for project ranging from building and testing instrument such as spectrometers and cameras to larger structures such as telescopes to large volume metrology and alignment at the observatory level for spacecraft payloads [2]. The group boasts a full complement of alignment tools including laser trackers, laser radars, interferometry, theodolites, portable metrology arms, and the first cryogenic photogrammetry system to operate down to 30K.

One of the projects that involved the support of the AI&T group was the OSIRIS-Rx Visual and Infra-Red Spectrometer (OVIRS) for the Origins-Spectral Interpretation-Resource Identification-Security-Regolith Explorer (OSIRIS-Rex) mission (section 3.0). The purpose of this report is the outline the tools, methods, and approaches to metrology utilized by the AI&T group and how they were applied specifically to the optical alignment of the elements on OVIRS during the ambient I&T phase.

1.1 BRIEF OVERVIEW OF METROLOGY INSTRUMENTATION

Laser Radar is a non-contact Cartesian coordinate measuring machine that uses a sensor to direct a focused invisible infrared beam to a point and coherently processes the reflected light [3]. The laser radar has different measurement mode that allow for multiple metrology methods to provide information. The laser radar can log single point measure by shooting metal tooling balls placed in a target location, or it can provide multiple points to provide a surface or an envelope by scanning an object. The radar can interface with the program Spatial Analyzer™ which enables real time analysis of the data as well as the ability to best fit the current data to information gathered from other instrument or the same instrument, but in different locations.

Laser Tracker like the laser radar is a non-contact Cartesian coordinate measuring machine. This machine has and internal distance measuring interferometer (DMI) and an external spherical magnetic reflector (SMR) to measure absolute and relative location in space. The laser tracker find the center of the SMR and has the ability to log a single point in space or multiple points by follow the SMR being trammed across a surface. The tracker has the ability to operate in two different modes: Automatic Distance Meter (ADM) which allows for the beam to be broken, and (IFM) in which the beam must not be broken or the SMR must return to the home position and start over [4, 5, 6]. Laser trackers also interface with the Spatial Analyzer™ software as well.

Auto-collimating Theodolites are useful in determining direction vectors off of mirror surfaces. The reticle of the theodolite has and illuminated crosshair that is reflected of a flat mirror surface. When the reticle is co-aligned with the optical axis of the mirror normal, the illuminated crosshair will appear aligned with a crosshair that is in the eye piece for the theodolite. The theodolite has both a rough and fine adjustment about the vertical rotational axis (azimuth) and the horizontal rotational axis (elevation). The positional readout for the instrument is coincidently the same. One theodolite can be used to determine a single surface normal or a network of theodolites can be used to collect data on multiple surfaces and transform to a common coordinate frame through an analysis program known as Optical Alignment Facility Data Analysis Macros (OAFDAMs) [7, 8, 9, 10, 11].

Micro-Vu For smaller systems and components, digital microscope-type metrology instruments offer an accurate, non-contact solution [12]. They can be used to centroid on various types of features such as machined holes, metrology targets, edges and a multitude of other targets, including optical surfaces and large-format detectors. The advantage to these systems is that they are highly accurate (on the order of a few tens of microns at worst). Another advantage is that they can be used for electronically- and contact-sensitive parts such as detectors and MEMS devices. A few disadvantages are the limited measurement volume and the line of sight limitations of having to look down at the part on the platen surface.

Figure 1-1. Micro-Vu in the cleanroom.

The Micro-Vu was used for OVIRS to measure detector fiducials with respect to metrology targets on the assembly housing and the mechanical interface before integration to the instruments. In this case, the detector assembly incorporated measureable features that were used at the subassembly level and after installation to the flight bench. The Micro-Vu system measured those features, along with the detector fiducials on the array. This information was used to calculate the shim dimensions to place the detector at the science instruments predicted focal surface.

1.2 INTRODUCTION TO UNCERTAINTY

In conducting the metrology to assist in the alignment and verification of ISIM, each measurement is effected by some degree of uncertainty. The instruments used for all of the measurements have their own uncertainty that can be represented as range attributed to the measurement noise. The amount of acceptable uncertainty for a given measurement can very base upon the type of measurement taken, whether it's a system measurement and there is a stack up of uncertainty, or an individual component that corresponds direct to the instrument uncertainty. These uncertainties drive the measurement and analysis for JWST ISIM. "Student's T" is a method of data analysis used by the alignment, integration, and test group at NASA Goddard and is used in the data reduction for ISIM. Another technique applied to the data using the Spatial Analyzer software is Unified Spatial Metrology Network (USMN), a method used to help with analysis and characterization of equipment uncertainty for networks of instruments [13].

2.0 METROLOGY INSTRUMENTATION AND MEASUREMENT TECHNIQUES

In the first section, I provided a brief description of the instrumentation used in the optical I&T process for OVIRS. This section of the paper will be an in-depth description of the three primary metrology instruments that are used to mechanical align the optical systems. The laser radar and trackers are used in conjunction with theodolites to provide information on system and component level as built positions and pointing vector as well as track rotations and translations that may occur during the metrology evolution of the project. This section will outline and explain the theoretical framework behind the function of each instrument, the various types of modes for data acquisition, the measure technique and routines that apply to the work in the optical AI&T group, and the software that we use to interface and analyze the data.

2.1 LASER TRACKER

The LT is a non-contact 3d Cartesian coordinate measuring machine that tracks the motion of retro reflective targets. This machine is highly useful in establish coordinate systems for the alignment and integration of the science instruments onto the ISIM structure. Due to the ability of the LT to conduct non-contact measurements, it affords us the opportunity to measure a wide range of structures in various configurations. Measurement capabilities of the tracker include the ability to record data through windows as well measure target through fold beam path in the event a fold mirror is required. This section will explain how the LT operates and to classify the two specific modes that the LT operates in to measure targets.

The LT operates simply by measuring the angle and the retro reflective target by reading reflect light on the return path through the re-entering the machine. The tracker head shot a laser that operates on drive motor on a gimbal mount with two mechanical axes, azimuth (angular) and elevation (or zenith). There is encoder on in the drive head that provide the angular readout out for the position of the retro reflector. LT's determine the distance in one of two methods: Absolute Distance Meter (ADM) or Distance Measuring Interferometer (DMI). The most common retro-reflective targets used in LT measurements are Sphere Mounted Retro-reflectors (SMR). The SMRs come in fixed radii known be the LT's operating software (SA^{TM} in this case) allowing for a constant offset to be accounted for giving the correct coordinate for the point in space. Some alignment fixtures for the ISIM structures also used solid glass retro-reflectors (SGR).

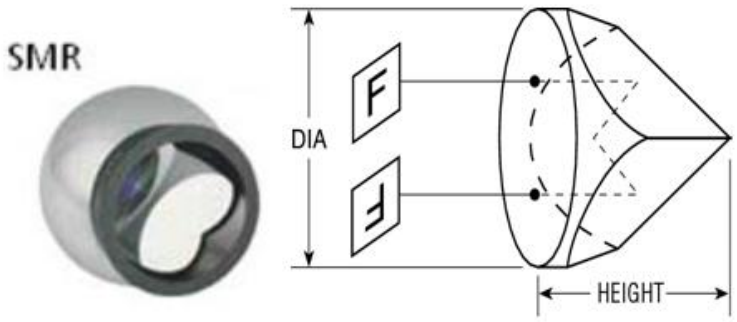

Figure 2-1. Spherically Mounted Retroreflector

2.1.1 Measurement Modes

The measurement uncertainty associated with DMI is typically around 5 microns (1-sigma) with an additional 10-15 microns associate to each additional meter both in the horizontal and vertical DOF with respect to the orthogonal to the range direction the LT. The 1-sigma uncertainty is increased to roughly 25 microns in ADM mode. SMR's consist of a corner cube machined into a precision tooling carefully making sure the apex of the mirrors coincide with the center of the tooling ball.

2.1.1.1 Absolute Distance Meter (ADM)

ADM, as stated above, is less accurate than measuring in DMI, however ADM is the more efficient mode. The LT does not require a known starting position in ADM mode because the LT uses a proprietary time of flight technique to calculate the position of the SMR. An infrared light from a semiconductor laser reflects off the SMR and returns back into the LT, where the returning light is converted into an electrical signal. This signal is analyzed by electronic circuitry that is encoded with the time of flight algorithm which multiplies the value by the speed of light in air. The refractive index of the air can be effect by the climate of the surrounding area, therefore the SA software allows for alteration the temperature setting provided by the portable whether station that is kept with the LT station. This is the most effective and time efficient mode for measurement and is well suited for bulk metrology. We operate in this mode because we are able to equip the ISIM structure, ITP, and the alignment fixtures with magnetic SMR nest in which we can populate simultaneously with targets. All the time that is gain in the measurement process come from the ability to use the drive motor in the LT head to point and shot at each target versus manually hopping targets from point to point while trying to keep continuous contact between the beam and the SMR.

2.1.1.2 Distance Measuring Interferometer (DMI)

DMI is an incremental measurement mode based on built-in interferometer and a frequency stabilized Helium Neon (HeNe) laser. The LT works on the two beam interference principle to establish the distance between the SMR and itself. A reference beam goes directly into the interferometer directly while a second beam actually leaves the LT, reflects of the SMR and return into the interferometer. The two beams interfere with each other showing a cyclic change in the interference fringe pattern observed by the sensor inside the LT. The electronic circuitry counts the change in cycle to determine the position of the SMR. To measure point in DMI, the SMR must begin at a position that may set arbitrarily by the operator. The default location for the home position is a nest located on just below the drive head of the LT. This default homing point for the tracker is also known as the "bird bath." Once the home is set position is measure and set by the LT, an operator will then walk the SMR to the target location to measure without breaking contact between the beam and the SMR. If the beam is "broken," the measurement is disrupted and the operator must start over from the home and begin again.

2.1.2 Tracking

The LT does have some features that have proven useful during the alignment process that is attributed to the tracking functionality. For certain fine alignment procedures that require placement of mounts or nests and rowbusted fixture that require shims, SA's ability to import coordinate frame and reference values can be used in conjunction with the "watch function" in SA. The watch function allow the operator to select a target value already in the work space as a reference value. The LT is locked on to an SMR and will track the position of the SMR in comparison to the reference value selected. A window will pop up on the screen showing a constantly update delta between the actual position of the SMR and the reference value in SA. As the SMR moves the delta will reflect the movement allowing one to visual walk, shim, and lock down an object into the desired position.

The tracking ability of the LT also has a feature that will continuously record measure point to a single point group of a moving target. We call this "tramming" a surface. In the SA window, the operator will change the acquisition move to a spatial scan. The LT will the lock on to the SMR's initial position as the initial point in the group. The operator then can move the SMR and the LT will measure point along the motion of the SMR as long as the SMR and the beam don't break contact.

2.2 LASER RADAR

The LR is similar to the LT in the sense that the LR is also a non-contact 3D Cartesian coordinate measuring tool that has a motor driven head that rotate about two axes (Azimuth and elevation). The LR is a direct energy instrument that conducts range measurements based on LIDAR (Light Ranging and Detecting) Like the LT the LR utilizes optical path length correction base on the index on the air, but the LR relies on scatter (mechanical) and specular (optical) returns to either scan surfaces to create envelops or measure single points by finding center of specular convex tooling balls. The beam path is split between the light leaving the instrument and a reference path through calibrated optical fiber that is housed in an environmentally controlled module. The reflected light re-enters the module and recombines with the reference beam to lock down the absolute distance. Due to a large laser modulation bandwidth (100 GHz), the LR can make precise measurements in milliseconds. The instrument used a visible red laser (660 nm) in unison with a camera on the drive head with the ability to adjust focus to allow the operator to view the surface to be measure through SA. A second infrared beam is used to make the measurement.

This instrument is the main tool used in the bulk metrology process for measuring the ISIM structure, the science instruments, and the alignment fixtures. Though the LT and the LR are both non-contact CMM instruments, the LR provides a far improved ability for automation during a measurement run. A large abundance of tooling balls in comparison to a limited quantity of SMR's allows for an entire structure to be prepopulated with targets. A single operator is able to use the drive motor in the LR head in conjunction with the camera to record each tooling ball location from the computer operating station attached to the LR as oppose to the need for someone to physically "hop" the SMR from location to location on the instrument structure. LR also has an automatic measurement feature that allows the operator to pick a nominal measure group of points as reference for the LR to automatic point at to complete entire measurement sweeps. The LR is the most versatile of the metrology equipment used in optical metrology for the spacecraft hardware and GSE. The instrument limits labor, increases safety, and show a combination of speed and accuracy. The figure below is a table that illustrates the comparison of the LR to other metrology instrumentation.

Table 2-1. Metrology Tools

	Photogra-mmetry	*Theodolite*	*CMM*	*Structured Light*	*Portable Arm*	*Laser Tracker*	*Coherent Laser Radar*
Portable	Yes	Yes	No	Yes	Yes	Yes	Yes
Fast Setup	No	No	No	No	Yes	Yes	Yes
Fast Relocation	No	No	No	No	No	Yes	Yes
Any Lighting	No	No	Yes	No	Yes	Yes	Yes
Climbing Risk Eliminated	No	No	No	No	No	No	Yes
Noncontact Advantage	No	No	No	Yes	No	No	Yes
Targeting Eliminated	No	No	Yes	No	Yes	No	`Yes
Offsets Eliminated	Yes	No	No	Yes	No	No	Yes
Runs Unattended	No	No	Yes	No	No	No	Yes
Automation Integration	No	No	No	No	No	No	Yes
Very Large Volume	Yes	No	No	No	No	Yes	Yes
Highly Accurate	No	No	Yes	No	No	Yes	Yes
Fast	No	No	Yes	No	No	Yes	Yes

2.2.1 Type of measurements

The LR has different method for which it conducts scan of surfaces and record points. This instrument can log single points or an array points in which each point carries a complete set of data (metrology scan and fast metrology scan), or a massive number of point that are place into a point cloud (vision scan). The amount of time taken for each scan can vary based on the parameters of the scan set by the operator, but the scans differ from each other by the amount of detail. The scan time depends on the type of scan, the size of the area to be scanned, and the density of the scan.

2.2.1.1 Single Point

The LR has the ability to point and shot shoot single target positions and log the point location in SA. This function utilizes tooling balls that are a held in place by magnet nest that can be machined to be fit the desired structure under test. The magnetic nest allow for repeatability. The LR does a spiral scan of the tooling ball to find the peak spectral response. At this point the LR calculate the distance to the tooling ball based off a time of flight calculation. In order for a point to place at the center of the tooling ball, the radius has to be specified in the interface software to factor into the calculations.

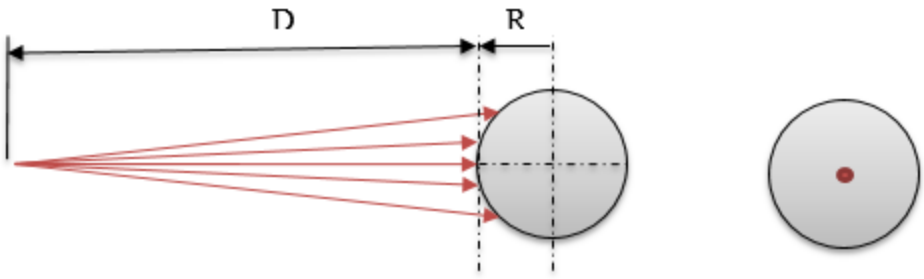

Figure 2-2. Laser radar point measurement of a tooling ball.

2.2.1.2 Vision Scan

The vision scan is the least detailed of the scan in the amount of information provided by individual point. Vision scans don't produce singular points with a three dimensional value in space in SA. Point from the scan are place into a point cloud and provide in which you can see a "cloud" of point create an envelope of the scanned surface. Despite inability to provide as much detail per single point as the other scans, vision scans take the least amount of time. This scan is preferable when scanning large areas and creating high density scans in a timely fashion.

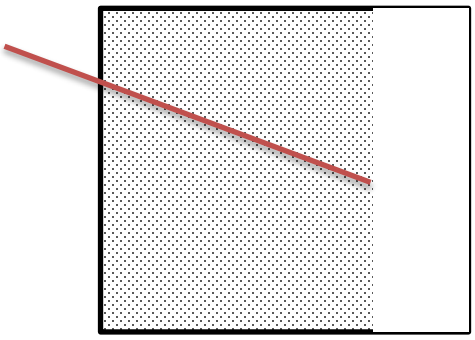

Figure 2-3. Laser radar vision scan box.

2.2.1.3 Fast Metrology Scan

A fast metrology scan is a more detailed scan than a vision scan. If the scan were classified on a scale from basic to advanced, the vision scan would be a basic level scan and the fast metrology scan would be the intermediate. This scan does not place point into a cloud like the vision scan; the fast metrology creates individual point in SA that have three dimensional values. An area to be scanned (scan box) is defined in SA and then second set of parameter known as the line width and the line spacing a set. The radar creates a point by scanning along a line of a set width into SA and the software then creates a point by averaging the information

taken along the line. The scan box determines the area under test while the number of recorded point and the density of points over the surface envelope are determined by the line spacing. The envelope of points created in SA is the same as the envelope create by a metrology scan. This scan takes more time than a vision scan, but less than a metrology scan. The advantage to using a fast metrology scan with more detailed information cut down on some of the time it take to complete the scan.

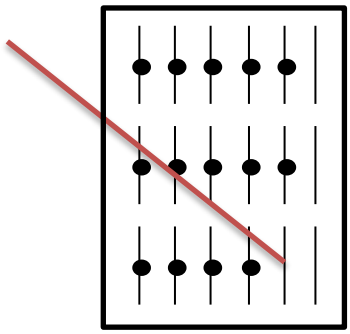

Figure 2-4. Laser radar fast metrology scan box.

2.2.1.4 Metrology Scan

The metrology scan provides the most detailed information per data point of all the scans. This scan requires the most time in general and has the largest amount of scan parameters. In looking at the figure below, there is a large box surrounding the whole area. This box is the scan box and it set the area to be scanned. The number of point and the density of the points that will make up the surface envelope will be determined by the box width and the line spacing. The radar scans the small are (the small scan box) and averages the data over the area to create a single point. The large scan box is populating by the smaller box scans according to the spacing and the width provided by the operator.

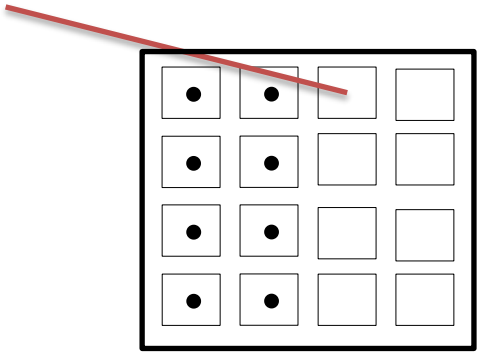

Figure 2-5. Laser radar metrology scan box.

2.2.1.5 Hole Scan

The LR has a routine that allows the instrument to create a point at the location of a hole in the system. This algorithm requires the operator have knowledge of the hole diameter and the size of the chamfer in the hole. Once the hole diameter and chamfer size are set, the operator must designate the number of "slices" the radar takes through the hole. This simply means the radar

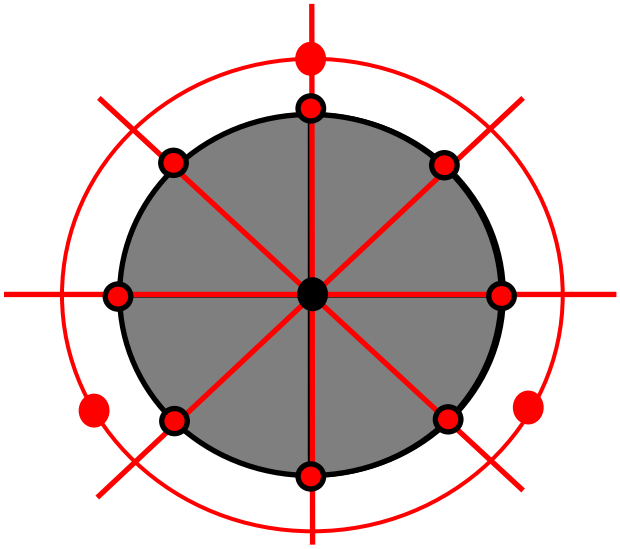

Figure 2-6. Laser radar hole center point measurement routine.

scans a straight line through the center of the hole after has taken three surface point measurement around the hole. The operator must also set what is refered as the clearance zone. This is another diameter that is larger than the hole in which defines where the three shot around the outside of the hole. Two edge points are taken along each slice. The figure below show a hole scan with the radar taking four sliced through the hole. The outer circle is the diameter of the clearance zone while the inner circle would be the hole diameter.

When performing a hole scan, the results can be effected by the angle in which the LR is viewing the hole. It is important to be as close to a normal incidence to minimize the uncertainty of the hole algorithm. As the incidence angle increases and becomes more oblique the LR begins see the hole vary in diameter depending on the orientation of a particular axis. The LR then begins to see the hole as more of and ellipse versus a circle, which can cause the algorithm to improperly fit a point to the hole or the algorithm could fail all together not producing a measured point.

2.3 MEASUREMENT ROUTINES: LASER TRACKER/RADER OPERATION

The LR and the LT are both 3D Cartesian coordinate measurement machines that are non-contact to varying degrees and rely on a time of flight calculations to measure the range of a target and read the azimuth and elevation base of encoder values. A lot of the operation of the instruments are very similar in the operator interface. As stated in previous sections, the tracker can only measure SMR's and in order measure planes, an operator must physically tram a target across the surface of the item to which the metrology is being perform. The radar measure a specular response making it completely non-contact. Each instrument can be used interchangeably with each other for a wide variety of jobs ,but an experienced operator with both instruments can discern which instrument will be better or more efficient for a given job based on the plus and minuses of the LR versus the LT. Some of the similar measurement routines between the LR and LT are there ability to measure items through reflective surfaces and further, through post processing, create the plane of surface in space allowing points to be fold about the axis of reflection.

2.3.1 Measuring Through Fold Mirror

Many optical systems include fold mirror to contain the optical path to fit the dimensions of the structure housing it. Optical alignment can prove difficult in these situations because the optical path length is hard to define couple with a not well-defined axis for the system. The LT/LR can alleviate the difficulty in measuring and aligning components in the system. If one of these instruments are placed in a position such that the laser can follow the same optical train as the system design, the instrument will measure the position of the reflected image and place the point in SA according to the OPD.

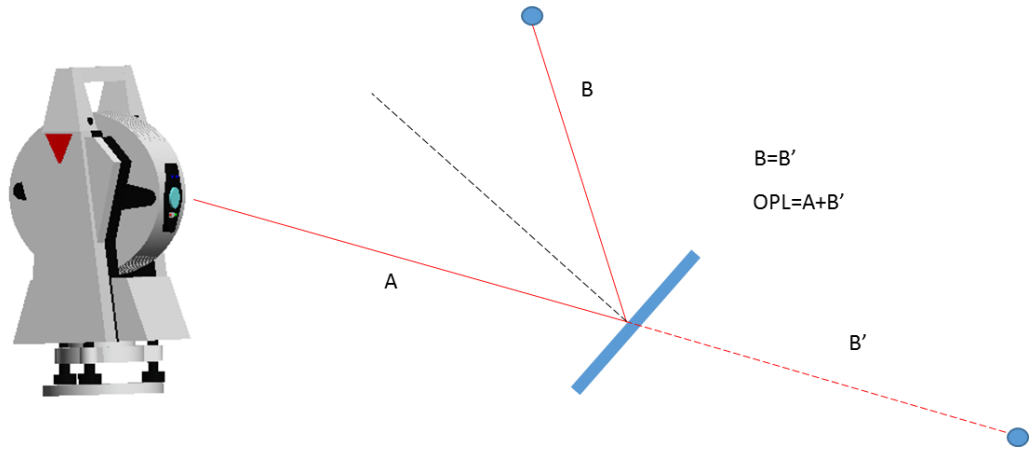

Figure 2-7. Laser tracker measuring a point through a fold mirror.

Figure 2-7 illustrates a LT measuring a point through a fold mirror. As stated above, the LT and the LR does not see the point as an object reflected about a plane, but rather as a point in space as if the mirror was not there. Consequently instead of seeing the point as the measure target at the end of *B*, the instrument see an imaginary point at the end of *B'* the instrument only sees the OPL as according to the time of flight calculation. The point is then read out at the end of the line the instrument is reading from the encoders for the azimuth and elevation values. The engineer can then use a technique to define the mirrored surface as a plane in SA™ allowing him/her to fold the fold the point in space in post processing, visually replicating the system. This technique as a "Direct and Through" measurement [14].

2.3.2 Direct and Through

A "direct and through" (D&T) measurement is simply what the name suggests. A SMR of tooling ball is places in a position such that the instrument used at the time can see the target both directly and through the mirror. This measurement routine is illustrated in Figure 2-8 below.

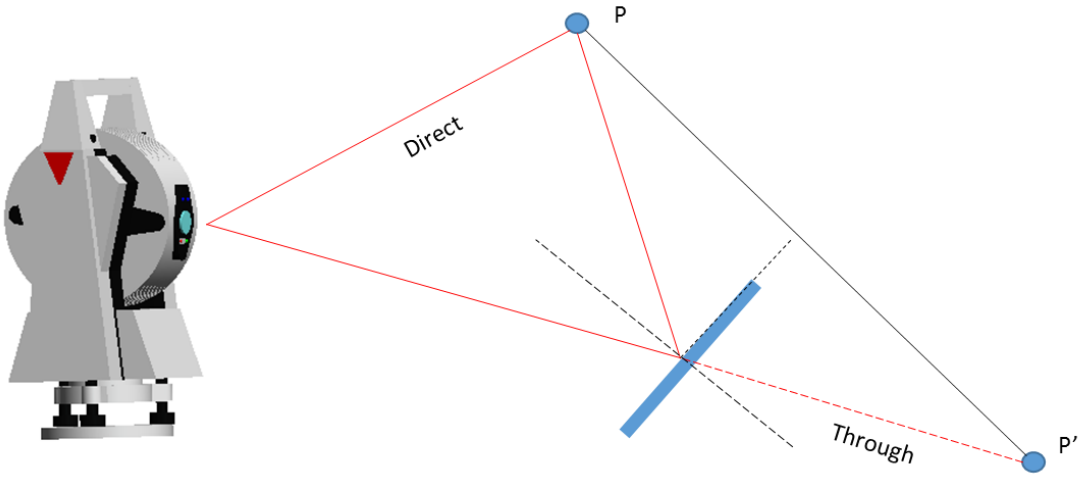

Figure 2-8. Laser tracker "Direct and Through" measurement routine.

The instrument then takes the direct measure and the measurement of the target through the mirror and places the two points into SA. SA has a command on the construct plane options that requires the operator to select the instrument station and the two point call "Mirror form two measure points." This command will construct the plane of the mirror with respect to the system according to the coordinate frame the operator has deemed active in the program.

2.4 SPATIAL ANALYZER™

SA is graphical 3D metrology software developed by New River Kinematics that has the ability to communicate with a vast number of 3D measurement systems [15]. During rounds of metrology, this software is used to simultaneously operate the LT and LR as well as conduct preliminary analysis of data during the actual measurement run. The post-metrology analysis is conducted using SA as well. The software is compatible with software tools that allows for the import and export of files such as MS office files, CAD models (IGES, STEP, VDA, SAT, and etc.), HTML, and more. Analysis done in SA can be easily tied into the analysis done in the other software that we use to combine the metrology data from the LR/LT with the data taken via the theodolites. SA was also used conjunction to analyze and reduce data with V-STARS to complete the analysis of the PG data.

The base functions of SA include the advance technologies for analysis and precision and computations as well as a multitude of tools for edit visualization, construction and analysis. SA allows us to do analysis on relationship fitting by giving us the ability to compare and transform points to points, points to objects, objects to objects, and even construct multiple coordinate frames that can be transformed as well. Mass number of points can be recorded and place into point clouds or single points with a significant amount of information can be recorded. SA also has the ability to calculate and classify the uncertainty that corresponds with the measurements of the data in the program. Unified Spatial Metrology Network (USMN) is the function in SA that helps classify the uncertainty of measure and is a term that will be used frequently in this paper in the speaking about the analysis process.

2.4.1 Best Fit Transformation

The LT and the LR both have a "cigar-shaped" uncertainty profile to each measured point. The instruments have a tighter uncertainty profile in the transverse axes of the beam in comparison to the longitudinal direction. Typically when metrology is performed on a given task, it is best practice that each target is shot from a minimum of positions (each position is referred to as a station) with the LT and the LR in order to establish the most accurate point in space in SA. The multiple stations are for the purpose of the USMN function in order to minimize the uncertainty. Each time an operator moves an instrument to a new position, the operator must go into SA and shut down the interface from the previous station and add a new

instrument to the file. SA's by default always places the new instrument at the origin of the active coordinate frame in the file.

In order for the placement of the each measured point in SA for the multiple station to correspond to each other on a universal coordinate frame, the operator must use what we refer to as "Tie Points." These points don't necessarily have to be located on the object of interest, but can be place around the object as well. These points however must be lock down and rigid because the operator must make sure that these points do not move as they are measured by each station. The tie points are used perform a "Best Fit Transformation."

When performing a Best Fit Transformation, the operator begins be completing a full sweep of measured point for all the points on the object or structure that can be seen by the LR or LT for that specific station. Once the LR/LT is moved to the next station, the operator then measures the tie points (minimum three), allowing him to transform that instrument's coordinate frame to the frame established for the system under test. In general, when performing a best fit transformation, one want to choose points with the largest spread between distance and variation of height if possible in order to lock down as many degrees of freedom as possible.

During the integration flow of a given project, there will be multiple configurations as elements are integrated to a housing or a structure. Depending on the size of a project and the type of test that can occur over the life of an integration cycle such as vibration testing, cryogenic testing, acoustic testing and many more that can vary from project to project. Best-fit transformations allow engineers to complete data reduction and compare information from test to test during the life of the I&T flow. For example, if there is a bare structure and in instrument is to be integrated, the metrology engineer would use the metrology instrument of choice to take a baseline round of metrology before the team begins the integration of the instrument. The team would then integrate the instrument to the structure and then another round of metrology would occur.

The data will then be reduce and analyzed to compare the structure pre-integration to post-integration. In order to know if there were any changes to the structure, the data collected during the metrology must be in the same reference frame for the pre- and post-integration metrology. There are certain targets on the structure that would be best fit to establish value in the correct reference frame, reorienting the structure in SA resulting in the metrology data

corresponding to the correct vales in the vehicle coordinate system. SA will generate a report showing the translation and the rotation that take place in order to complete the transform.

The next thing that would be examined in the post integration metrology is the placement of the instrument. By applying predictions, a model can be developed with reference values for the instrument. Best-fitting into to the value from the previous configuration and entering the coordinate frame, a quantitative judgement on the place of the instrument can be made.

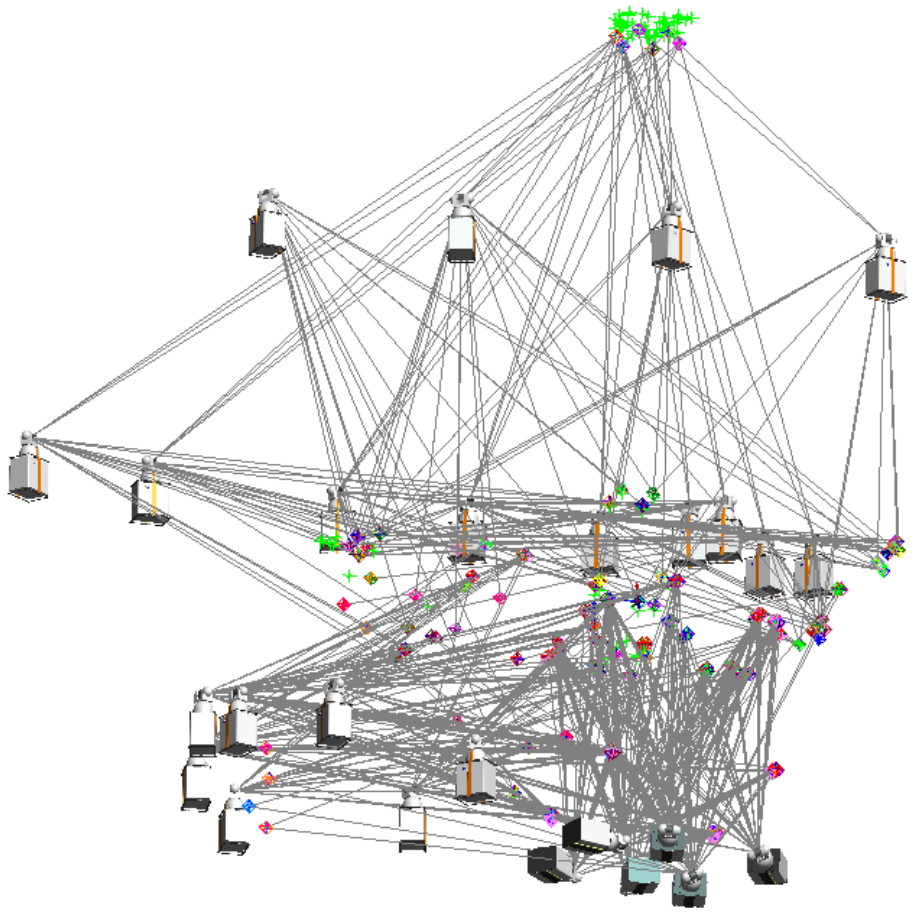

Figure 2-9. Laser Radar survey of the James Webb Space Telescope's Optical Telescope Element.

The figure above is a LR survey of the James Webb Space Telescope's (JWST) Optical Telescope Element (OTE). As a rule of thumb, it is best to measure every target of a given metrology run from a minimum three stations to help minimize the uncertainty of the point measure via the USMN. It took 24 LR stations to complete the survey of OTE.

2.5 THEODOLITES

One of the essential metrology instruments in the optical metrology and alignment process are auto-collimating theodolites. Theodolites are used to determine the orientation and envelope of critical components and optical boresight of spaceflight hardware. The components can be science instruments, mirror element, thrusters, and etc. Techniques used for spacecraft hardware are commonly used on critical ground support equipment (GSE) as well. This section will speak to the operation of the theodolites, the measurement process and techniques, and the data reduction and analysis.

A theodolite is essentially a telescope that is mounted on multiple rotational axes allowing for the instrument to point in any direction within the mechanical limits of the instrument. There are two rotational axes to be exacted. The telescope rotates 360 degree about the azimuth circle (rotation about the vertical axis) of the instrument. The elevation circle (rotation about the horizontal axis) does not have a full 360 degree rotation due to mechanical restrictions. When a theodolite is leveled to gravity, the elevation circle of the instrument will coincide to the gravity vector. If the theodolite is pointed directly up resulting in the telescope pointing to be antiparallel to gravity, the elevation reading should be 0 degrees. If the telescope is pointed such that the telescope pointing is perpendicular to gravity, the elevation reading will be 90 or 270 degrees (The convention used depends on the type of theodolite. At GSFC, the Kern DKM3 and Wild T3000 are the predominate theodolites) [16]. This is important because if there is a network of theodolites and each theodolite is leveled to gravity before a measurement is recorded, every theodolite in the network will have a universally have gravity as the reference for the elevation reading.

Measurements with the theodolites can be taken in unison with LR or LT measurement and transformed into a common coordinate system to provide positional and rotational orientation of the structure under test. The theodolite is used to determine the pointing vector of a mirrored surface based on auto-collimation. A projected image of a cross-hair is fixed at the focal plane of the theodolite telescope, while the focus of the telescope itself is set to infinity. When the optical axis of the theodolite is aligned to the surface normal of the mirror (perpendicular to the mirror surface or antiparallel to the surface normal) the reflected of image of the illuminated crosshair will be in alignment with the crosshair etched into the theodolite

reticle. The theodolite will be said to be in auto-collimation when the reflected image is aligned to the reticle upon adjusting the azimuth and elevation.

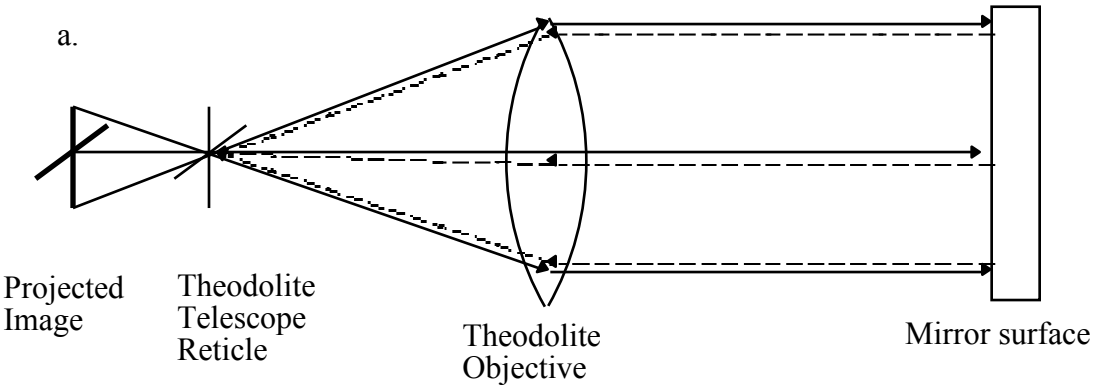

Theodolite optical axis perpendicular to mirrored surface-
"In auto-collimation"

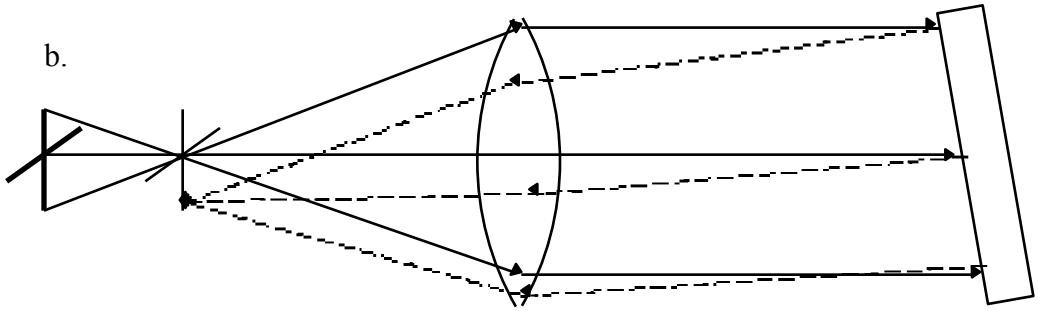

Theodolite optical axis not perpendicular to mirrored surface,
reflected image not on theodolite telescope reticle

Figure 2-10. Auto-collimation of theodolites [8].

Earlier in this section, it was mention that the boresight, instrument pointing vector, as well as the surface envelope can be determined using theodolites. The primary target used for the theodolites at GSFC are 2.0- or 2.5 cm cubes. These optical cubes can be made of metal or glass and are manufactured such that all the adjacent face are perpendicular to within 10 arcseconds. Flight structures and alignment fixtures have mirrors and optical cubes fabricated into them for the purpose of conducting optical metrology for the integration and testing process. During theodolite measurements, two adjacent faces of the theodolite cubes must be measured in order to determine the pointing vectors. The directionality of the pointing vector orthogonal to the measured surface normal of the adjacent faces, A and B, can be determined by the cross-product of the measure adjacent faces: A x B=T.

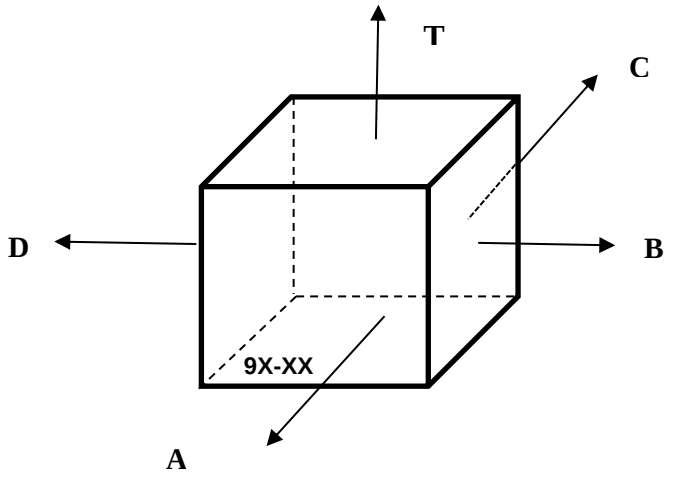

Figure 2-11. Optical cube face convention [8].

Recorded measurements of these optical cubes or CFMP's in the case of ISIM, are taken with respect to the spacecraft coordinate system. An ideal coordinate system will have an orientation such that the +X is pointed down (to coincide with gravity) and the +Y or +Z axis parallel to a side or major component of the spacecraft structure. In optical alignment, it is has proven helpful to allow the +Z axis to be parallel to the optical axis of the system. Rotations about the X-, Y-, and Z-axis are describe in term of roll, pitch, and yaw respectively. Zenith is the angle that describes the departure from the X-axis and is always between 0 and 180 degrees.

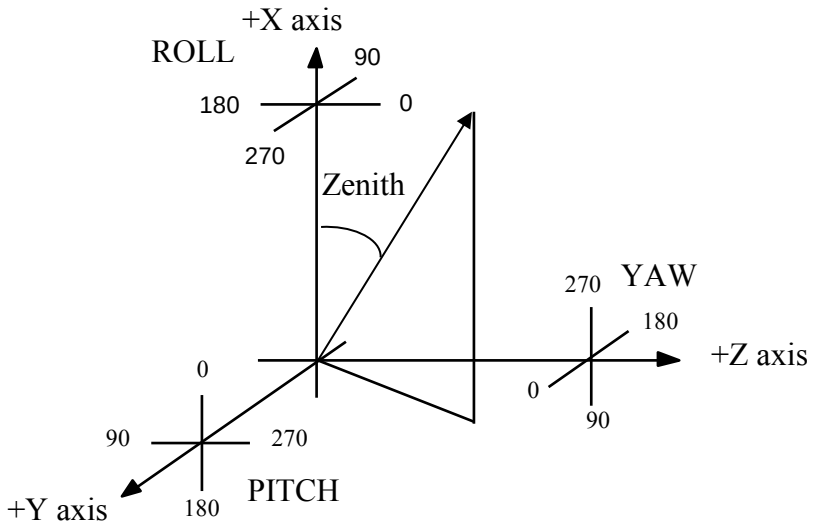

Figure 2-12. Schematic showing OAFDAM coordinate system definition and angle nomenclature [8].

Based on this coordinate system, any pointing vector can be described by a combination of two angles. Roll and zenith values are convenient for describing the pointing vector of a given target because those angles correlate directly to the theodolite's azimuth and elevation reading in a gravity based system. The zenith relates directly to the elevation reading while the roll value describes the azimuth value. Zenith and roll values become inadequate for describing a pointing vector when the vector is close to parallel to the X-axis. When the angular departure from the X-axis is $<45^0$ or $>135^o$, small changes in direction will result in large value changes in roll causing it to become indeterminate. I these cases, the point direction would be described by a combination of the pitch and the yaw values.

In order to calculate the roll, pitch, yaw, and zenith of a given target, the Optical Alignment Facility (OAF) Coordinate system must be define. Since the OAF is a gravity based coordinate system, the starting point for the zenith is the gravity vector which is always pointed down. As stated earlier, by leveling all theodolite in the network to gravity within 2-arcseconds, the gravity vector become a universal reference for the elevation readings. The theodolite auto-collimating on an optical reference obtains a direct reading on the reference's orientation with

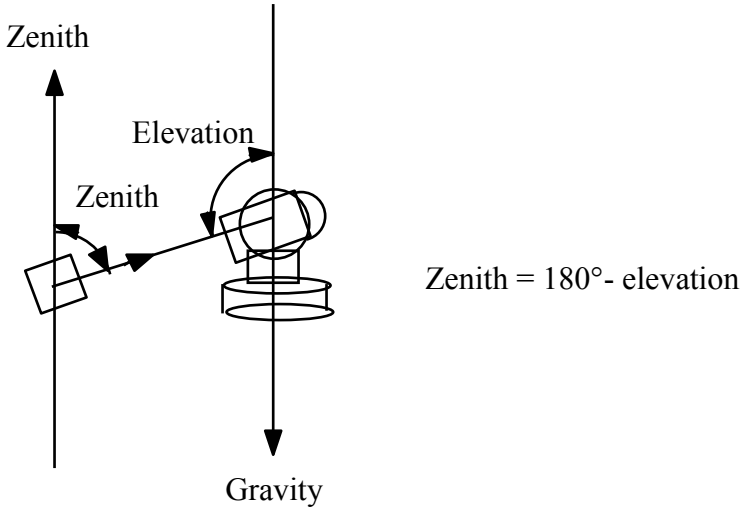

Figure 2-13. Theodolite elevation-zenith relationship [7].

respects to gravity. This results in a zenith value that is the complement to the of the theodolite's elevation reading.

In a network of theodolites, the roll reference for the azimuth readings are not as simple. There is no natural "world roll reference" such as gravity. A roll reference must be established for each measurement set. There are to main methods for establishing a roll reference: (1) placing a primary theodolite as the fix roll reference and (2) placing a standing optical reference from which all azimuth differences are measured. For the purpose of this paper, only the first method will be explained.

When there are multiple optical references to be used as targets for theodolites and multiple theodolites are used for the measurement round to create a network of theodolites, an OAF coordinate frame must be created. The primary theodolite is generally set up to auto-collimate onto one of the faces of the master cube for a given assembly. This theodolite should be positioned such that it has a line of sight to all other theodolite in the network. It is not always possible to have clear line-of-sight from the primary theodolite to all of the other shots. When there are a minimum of three theodolites, the orthogonal face of the master cube will serve as the reference for a secondary theodolite. These two theodolites should only rotated about their axes during a measurement set. Ideally, the theodolites should be positioned in the test such that all individuals involved can move freely with a minimum risk of accidentally "bumping" the primary or secondary.

A measurement theodolite is set to auto-collimate on a cube face, and the azimuth and elevation are recorded. The measurement theodolite is then bore-sighted to the primary theodolite, i.e. their lines-of-sight are placed anti-parallel to each other. At this point, the azimuths of the measurement theodolite and primary theodolite are recorded (termed the subject azimuth reference and primary azimuth reference, respectively). The geometry of the measurement forms a triangle, where the values of two out of three angles can be calculated directly from the subject azimuths and azimuth references. The third angle can be calculated, since the sum of all interior angles of a triangle is 180°. This third angle is the roll difference between the measured cube face and the primary cube face.

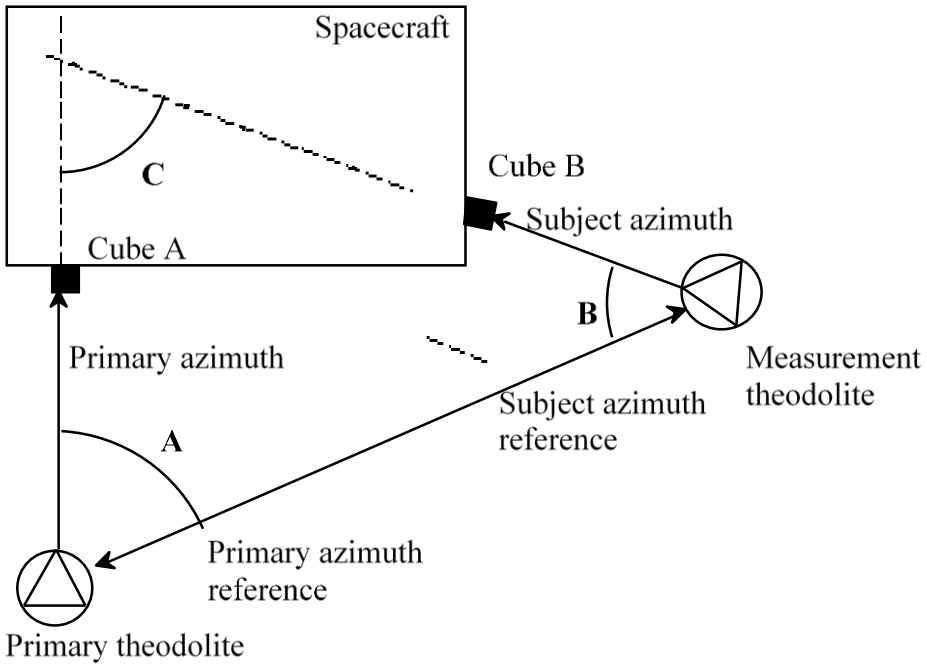

Angle A =primary azimuth reference - primary azimuth
Angle B = subject azimuth - subject azimuth reference
Angle C = 180° - (angle A + angle B)
= roll difference from the primary cube face to the measurement cube face

Figure 2-14. Primary theodolite as fixed azimuth reference [8].

In this system the OAF Coordinate is based at the center of primary theodolite. The roll value of any measured vector in the OAF Coordinate is given by:

Roll = 360-{(subj. az. - subj. az. ref.) + (prim. az. ref. + 180°)}.

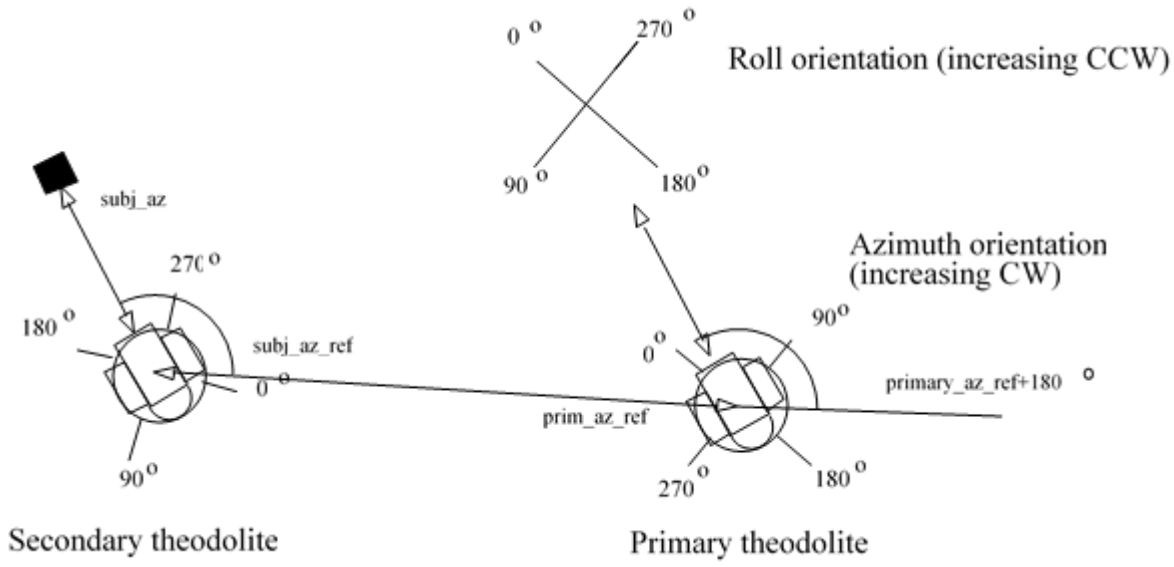

Figure 2-15. Calculating roll values [11].

Again, the '360-' term is used accounts because that roll increases counterclockwise while azimuth increases clockwise.

2.5.1 Data Analysis

Once all the alignment data have been reduced into the OAF Coordinate, the question remains as to how to get this information into a usable form. The problem with the OAF Coordinate is that one axis must be anti-parallel to gravity, and the coordinate system is centered in either the dihedral reference mirror or the primary theodolite. Further, the 0° roll vector is oriented in an arbitrary manner and not necessarily along any of the spacecraft coordinate axes. It is best to start with the simplest case: the spacecraft has been "levelled" which automatically places one axis of the spacecraft parallel to the +X axis of the OAF Coordinate.

Since the measured references are simply orientation vectors, they can be translated along the coordinate axes without changing their orientation. Imagine that the vectors are all translated so that their starting points are at the origin of the coordinate system.

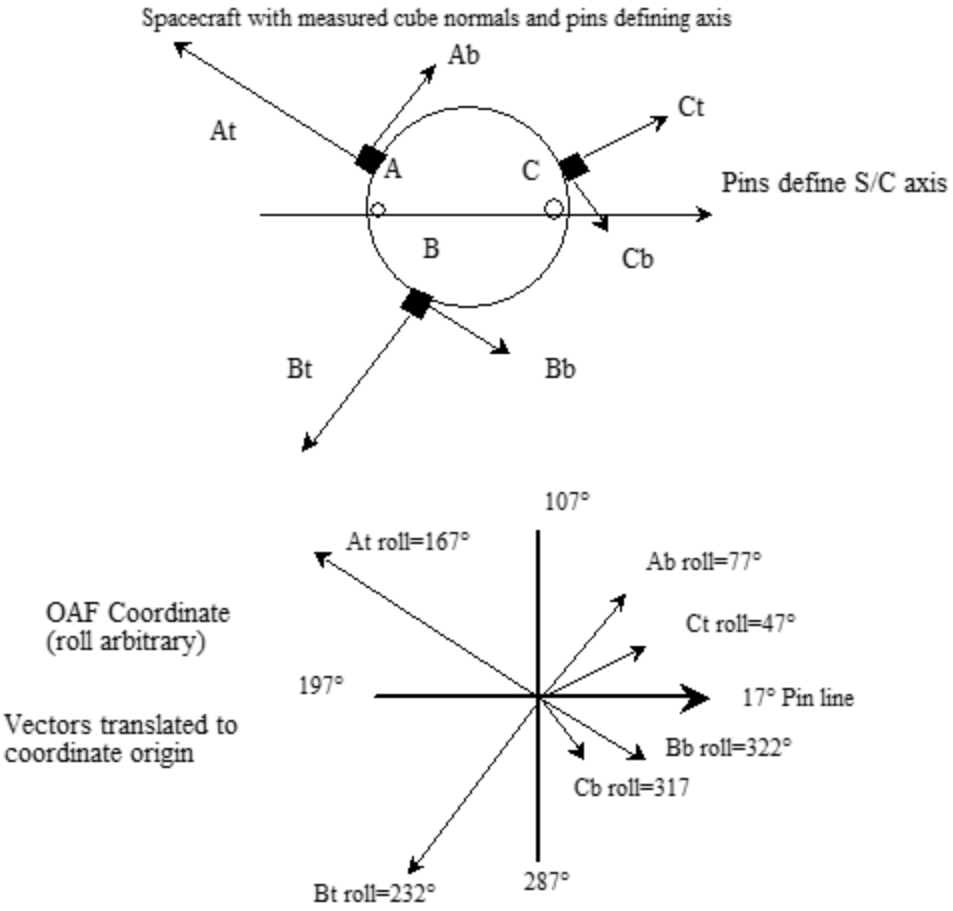

Figure 2-16. Vector translation to origin [8].

Since the present coordinate system still has one axis (the "up" axis) oriented parallel to the OAF Coordinate, the zenith values for these vectors do not change. Further, the coordinate system can be rotated about the +X axis a set amount without affecting the zenith values. The only result is that the roll value for each vector changes by the same amount, which again does not affect their relative orientations. Therefore, one of the horizontal axes, usually the +Z, to be set to a value of 0° roll (Figure 12).

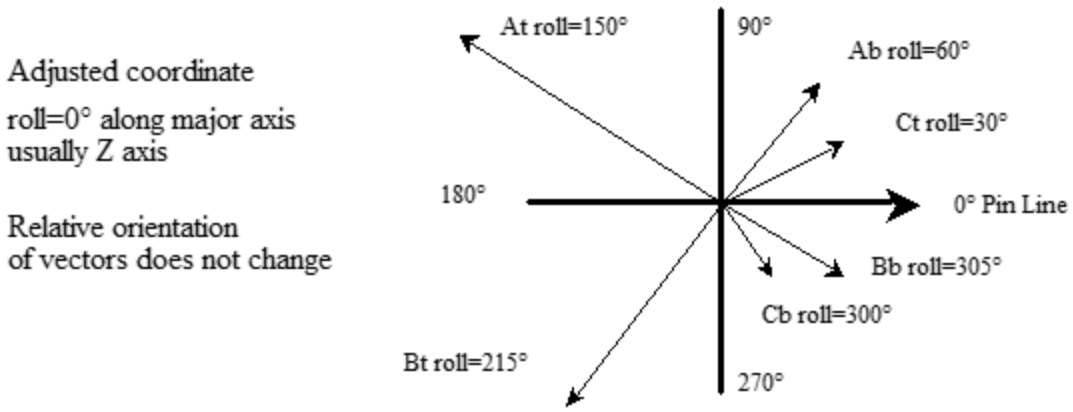

Figure 2-17. Coordinate system rotation [8].

For the simple case of the "levelled" spacecraft, this will complete the data analysis required to determine the cube face orientation in the spacecraft coordinate system. However, if the spacecraft +X axis is not conveniently located anti-parallel to gravity like the OAF Coordinate, each vector must be further analyzed into what are called "direction cosines". Direction cosines are the projections of the normalized pointing direction vector along each major axis. This means that each vector length can be set to any value with no effect on its relative pointing directions. So we can set each vector length to 1 (inch, foot, or centimeter, it doesn't matter). This process is known as normalizing.

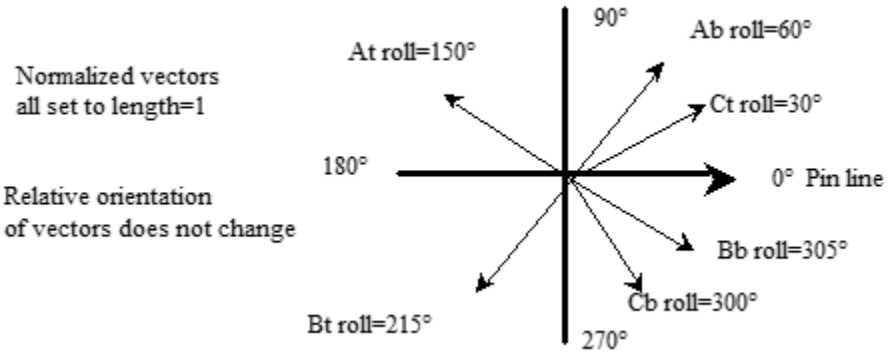

Figure 2-18. Vector normalization [8].

Since all vector lengths equal 1, the distance that each vector projects along any axis is equal to 1 x the cosine of the angle between the vector and that axis. For these vector projections, Mx2+My2+Mz2=D2 (Pythagorean Theorem) where D is the length of the vector or 1, and Mi is the direction cosine along the i axis (remember that the direction cosine is a distance value).

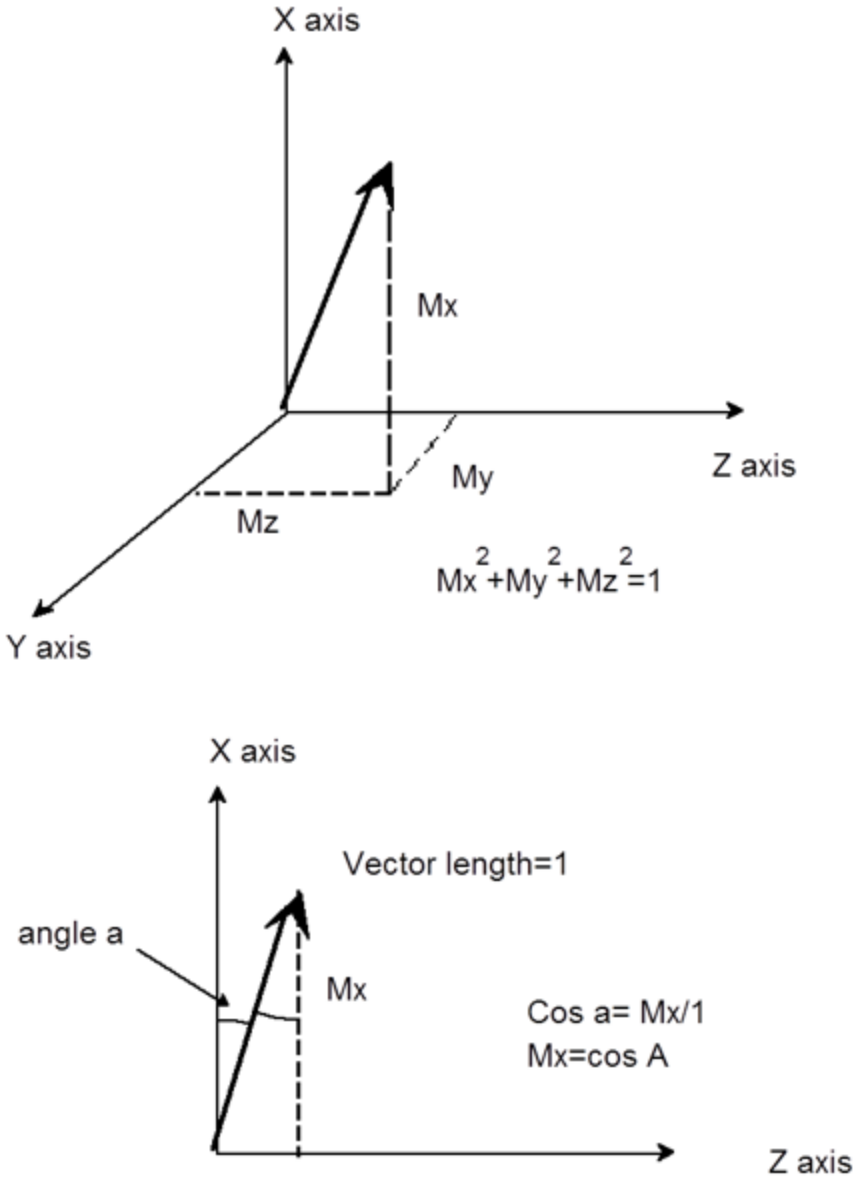

Figure 2-19. Direction cosines [11].

Direction Cosines can be calculated from roll and zenith values and vice versa (see Attachment 1). We now have a new way of defining the orientation of any vector, i.e.as a 1x3 array of numbers {Mx, My, Mz}. This matrix definition is convenient when the coordinate system must undergo significant transformations requiring the use of matrix operations.

At this point we have determined the relative orientations of all vectors in a coordinate system where the +X axis is still anti-parallel to gravity and the +Z-axis is horizontal and set to a roll value of 0°. By definition, in a right-handed orthogonal coordinate system, the Y axis is

perpendicular to both the X and Z axes (the cross product of the Z and X axes: Z x X = Y) and set to a roll value of 270°. Since the Y and Z axes are perpendicular to X axis, they have a zenith value of exactly 90°. We can thus define any vector in this coordinate system as a combination of roll and zenith values. Since the distance of each vector is one unit, we ara essentially expressing vectors in spherical coordinates (r, q,j) where r is always equal to one unit.

We can also determine the direction cosines of any of the vectors based on their roll and zenith values, since direction cosines can be considered as the corresponding cartesian (x,y,z) coordinates of any unit vector expressed in spherical coordinates. These direction cosines are especially convenient when the only transformations required involve changing the label or direction of the coordinate axes. For example, if the OAF Coordinate X axis becomes the spacecraft Z axis, the OAF Y axis becomes as the spacecraft -Y axis, and the OAF Z axis becomes the spacecraft X axis; analysis simply entails changing the order or sign of the respective direction cosines. In other words, set Mx (spacecraft) = Mz (OAF), My (spacecraft)=-My (OAF), and Mz(spacecraft)=Mx(OAF) or {Mx, My, Mz}spacecraft = {Mz, -My, Mx}OAF. The math is shown below:

$(Mx, My, Mz)_{OAF} \times A = (Mx, My, Mz)_{S/C}$

where A is the 3x3 matrix operator

$$A = \begin{pmatrix} 0 & 0 & 1 \\ 0 & -1 & 0 \\ 1 & 0 & 0 \end{pmatrix}$$

calculating the matrix:

The 1x3 array is transposed to a 3x1 array to facilitate matrix multiplication

$$\begin{pmatrix} 0 & 0 & 1 \\ 0 & -1 & 0 \\ 1 & 0 & 0 \end{pmatrix} \cdot \begin{pmatrix} Mx \\ My \\ Mz \end{pmatrix}_{OAF} = \begin{pmatrix} (0 \bullet Mx) + (0 \bullet My) + (1 \bullet Mz) \\ (0 \bullet Mx) + (-1 \bullet My) + (0 \bullet Mz) \\ (1 \bullet Mx) + (0 \bullet My) + (1 \bullet Mz) \end{pmatrix}$$

$$= \begin{pmatrix} Mz \\ -My \\ Mx \end{pmatrix}_{OAF} = \begin{pmatrix} Mx \\ My \\ Mz \end{pmatrix}_{S/C}$$

This analysis is sufficient for the simple case where we transform from the OAF Coordinate to the spacecraft coordinate by rotating the roll values to a known value and then interchanging coordinate axis directions. However, most spacecraft measurements are performed via a master reference cube.

When a master reference cube is attached to the spacecraft structure, one of the first measurements made during the alignment process is the spacecraft coordinate axes with respect to this master cube. The spacecraft is levelled to place one axis anti-parallel to gravity and a reference surface on the spacecraft is defined as another axis. In the example earlier, two alignment pins were used and the horizontal line from one pinpoint to the other defined this reference axis. The orientation of the master reference cube is then determined with respect to these axes. A transformation matrix can then be calculated that will transfer the direction cosines of vectors measured in the spacecraft coordinate system to a coordinate system defined by the master reference cube. Since the cube faces are manufactured orthogonal to each other, a coordinate system in the cube can be defined readily. The inverse of the transformation matrix from the spacecraft coordinate to the master reference will transform direction cosines from the cube coordinate system to the spacecraft.

Expressed mathematically:

A is the spacecraft to coordinate system transformation matrix (3x3 array).

$\{Mx, My, Mz\}S/C \bullet A = \{Mx, My, Mz\}cube$

$\{Mx, My, Mz\}cube \bullet A\text{-}1 = \{Mx, My, Mz\}S/C.$

We can now readily transform any vector measured with respect to a coordinate system defined by the master reference cube to spacecraft coordinates by operating (matrix multiplying) on it by the transformation matrix, A-1. This manipulation simplifies the measurement routines because the spacecraft no longer has to be levelled or even in the same orientation as the initial measurements. As long as the orientations of two faces of the master cube can be measured in the OAF Coordinate, the master reference cube coordinate can be defined and the spacecraft coordinate system calculated.

Determining this transformation matrix, A, is the next step. Transforming one coordinate system to another can be thought of as a series of three rotations, each around a major axis. The master reference cube face closest to the Z axis will have a roll value of R0 in the spacecraft coordinates as well as a pitch offset, P0. The face nearest the Y axis will have a yaw offset, Y0.

If the coordinate system is rotated by the opposite of these roll, pitch, and yaw offsets (i.e., by -R0, -P0, and -Y0), it is now based in the master reference cube.

The following matrix operators rotate coordinates:

Rotation of $-R_0$ about X axis

$$\mathbf{R} = \begin{pmatrix} 1 & 0 & 0 \\ 0 & \cos(-R_0) & \sin(-R_0) \\ 0 & -\sin(-R_0) & \cos(-R_0) \end{pmatrix}$$

Rotation of $-P_0$ about Y axis

$$\mathbf{P} = \begin{pmatrix} \sin(-P_0) & 0 & \cos(-P_0) \\ 0 & 1 & 0 \\ \cos(-P_0) & 0 & -\sin(-P_0) \end{pmatrix}$$

Rotation of $-Y_0$ about Z axis

$$\mathbf{Y} = \begin{pmatrix} \cos(-Y_0) & \sin(-Y_0) & 0 \\ -\sin(-Y_0) & \cos(-Y_0) & 0 \\ 0 & 0 & 1 \end{pmatrix} .$$

Vectors measured in spacecraft coordinates can be operated on in series by the matrix operators R, P, and Y. This can be a tedious process, but the rules of matrix multiplication allow the three operators to be combined into one matrix operator,

$$A = R \bullet P \bullet Y =$$

$$\begin{pmatrix} \sin(-P)\cos(-Y) & \sin(-P)\sin(-Y) & \cos(-P) \\ \sin(-R)\cos(-P)\cos(-Y) - \cos(-R)\sin(-Y) & \sin(-R)\cos(-P)\sin(-Y) + \cos(-R)\cos(-Y) & -\sin(-P)\sin(-R) \\ \cos(-R)\cos(-P)\cos(-Y) + \sin(-R)\sin(-Y) & \cos(-R)\cos(-P)\sin(-Y) - \sin(-R)\cos(-Y) & -\cos(-R)\sin(-P) \end{pmatrix} .$$

This is the transformation matrix for transferring vectors from the spacecraft coordinate system to the master cube coordinate system. (There are simpler and more mathematically elegant ways of accomplishing this result, but they are beyond the scope of this paper.) The

inverse of this matrix, A-1, will transfer vectors from the cube coordinate system to the spacecraft coordinate.

Therefore, any face vector of a component reference cube measured with respect to the master reference cube are operated on with the matrix operator A-1 to obtain that component cube orientation in the spacecraft coordinate system. In practice, a secondary reference cube is attached to the spacecraft structure and subjected to the same vector transformation procedure. This secondary cube serves as a backup if the master cube is separated from the structure or the line-of-sight to its faces is blocked. These matrices apply for transforming vectors in any coordinate system to any other, i.e., a transformation and inverse can be calculated from the OAF Coordinate to the cube coordinate, the master cube coordinate to secondary reference cube coordinate, or the secondary reference cube coordinate to the spacecraft coordinate.

Using the transformation procedure described, we can determine the alignment of spacecraft components to a satellite coordinate system via the use of optical cubes and autocollimating theodolites. The most important requirements are 1) to determine the component orientation with respect to its reference cube, 2) to determine the orientation of a master cube with respect to the spacecraft coordinate axes, and 3) to measure the orientation in the OAF Coordinate of at least two faces of each optical cube.

2.6 LASER RADAR, LASER TRACKER, AND THEODOLITES TIED INTO COMMON COORDINATE SYSTEM

Generally when measuring and optical system or a mechanical structure, theodolites are used in unison with the LR and/or LT for a round of metrology. Theodolites auto-collimating off of optical cubes or surfaces machined with an optical finish are the best method for characterizing the system rotations. The positional measurements that provide the information on translations in the system are provided by the LR/LT. Between the two methods of data acquisition, all six degrees of freedom have been locked down.

An individual instrument my typical have at least two optical cubes that are placed in a manor such that there is a significant spread between them coincidently driving down the measurement. Multiple tooling ball/SMR target nest are place in the same manor with a minimum of three nest to allow for best-fit transformations if the instrument is measured in different orientations. In order for the data to be sufficient in characterizing the system, the theodolite network most be in the same coordinate frame as the LT/LT network. This is accomplished via direct and through measurements.

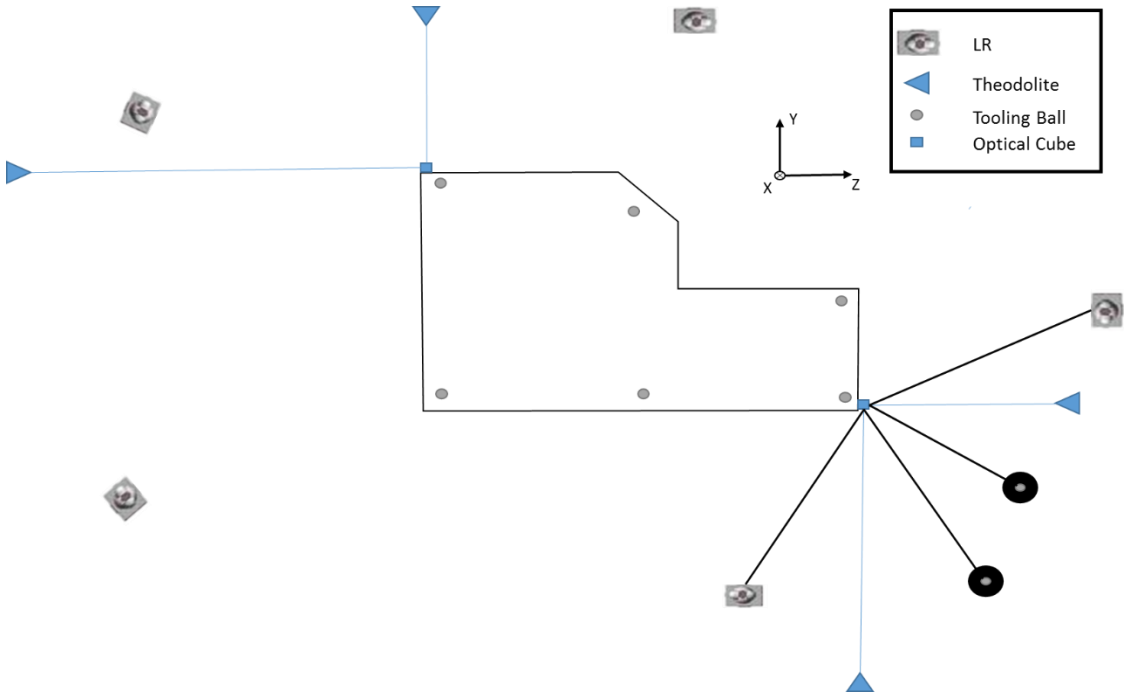

Figure 2-20. Generic metrology schematic.

In the figure above, there is an arbitrary, robust structure that will serve as an instrument for this particular case. The instrument has six tooling ball target place around the perimeter as well as two optical cubes. The optical cubes are attached to the instrument on opposite corners

to provide the largest possible spread between the cubes as explained earlier in the section. During the measurement run, the LR operator would measure all visible tooling ball targets with the LR. Each LR position is referred to as a station. The number of station used to measure a structure is up to the discretion of the operator. The rule of thumb for the proper amount of station for a measurement run is that each tooling ball target be measure from a minimum of three station for the USMN. The bigger the spread on the stations for each target produces the best results on driving down the uncertainty on the USMN.

In this test configuration, there would be four theodolites in the network used to measure the –Y and the +Z face of the primary cube and the +Y and –Z face of the secondary cube. As stated earlier in the paper, when two orthogonal face of a cube are measured the third direction can be determine by the cross product of the measured vectors. The figure shows two of the LR station doing a DT measurement of the primary optical cube on the same two faces shot by the primary and secondary theodolites in the network.

In the data analysis, the responsible engineer would first run a USMN on the tooling ball data in a new collection on the SA file entitle "Analysis." This point group then becomes the collection of points used perform all post processing of the data. If this measurement run is the very first measurement of the I&T phase, this group is best fit to nominal value pulled from a CAD drawing or some other mechanical design software. This then becomes the as measured reference group for future testing. If this measurement run if further down the I&T cycle such as pre-post vibe, cryogenic, acoustic, etc., then the USMN point group is best fit to the reference group set to be the as-bit measured reference and the compared to the previous measurement cycle.

Once the USMN point group has been created and best-fit to the reference collection in SA, the next step would be to create planes from the direct and through shot taken by the LR. (When post-processing data, whether it be constructing plane from a DT shot, lines from points, points from intersections, shape from scans of cloud points, and etc. it is best practice to complete these tasks after the USMN group has be completed and best fit to the reference data.) Two orthogonal planes are created in SA with their corresponding direction cosine determine by the active coordinate frame in SA. These direction cosines can then be exported to the OAFDAMs worksheet used for the theodolite analysis. The using the two faces of the primary cube to transform the OAF frame into the primary cube frame, the direction cosine from SA can

be then be use form a transformation matrix that transform the network from the primary cube frame to the instrument coordinate frame. The tooling ball data and the cube data are now in the same coordinate frame and can effective describe the system.

3.0 THE OSIRIS-REX INFRA-RED SPECTROMETER (OVIRS)

The Origins-Spectral Interpretation-Resource Identification-Security-Regolith Explorer (OSIRIS-Rex) is a NASA mission launched in 2016 to study the asteroid Bennu (RQ36) and return a sample to Earth for study in 2023 [17].

The OSIRIS-REx Visible and Infrared Spectrometer (OVIRS) is a spectrometer with a 4 mrad field of view (FOV) [18, 19, 20]. The instrument provides spectra of the surface of RQ36 over the wavelength range of 0.4-4.3 μm. It employs a faceted, wedged filter to separate the light (i.e., Linear Variable Filters; LVF). OVIRS spectra are measured with a resolving power R = 125 to 200 ($R = \lambda/\Delta\lambda$) over the entire 0.4-4.3 μm range, as well as with R = 350 ($\lambda/\Delta\lambda$) over 2.9-3.6 μm.

The alignment of the OVIRS instrument is an illustrative example of how opto-mechanical metrology tools and optical metrology techniques, such as interferometry, are used in concert to enable the accurate and fast construction of an optical system with little or no alignment-test iteration. It also demonstrates that large volume metrology instruments, like the laser radar and theodolites, are useful in the alignment of a "small" optical system, where reach-and-access considerations drive aspects of the opto-mechanical design, because they can work with smaller feature or target types with minimal human interaction. They also provide the flexibility needed for a one-of build where procedural details are uncertain. The OVIRS alignment is an example of not just a *precisely* aligned instrument (i.e., well-aligned internally for aceptable performance), but also an instrument that is *accurately* aligned (i.e., aligned in an absolute sense to a coordinate system, allowing accurate co-alignment to other OSIRIS-Rex instruments and the spacecraft coordinate system by the spacecraft integrator.

The system for OVIRS is comprised of two off axis parabolic (OAP) mirror, a primary with a clear aperture of 80mm diameter and a secondary with a 26mm clear aperture. These OAPs form what is essentially an afocal beam reducer with a field stop placed at the focus point between the mirrors and the entrance aperture ahead of the primary mirror.

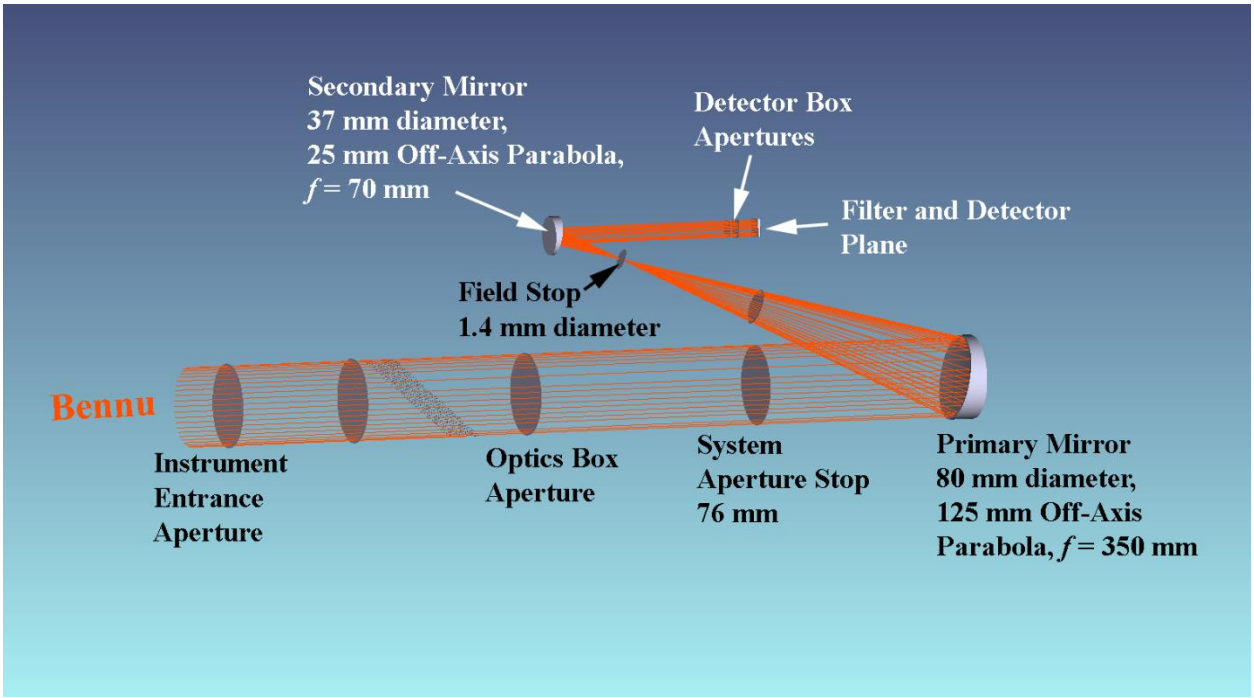

Figure 3-1. Ray trace of OVIRS optical system.

3.1 ALIGNMENT PHILOSOPHY

The OVIRS alignment steps and related data analysis and I&T evolutions are shown as a flow chart in Figure x. The assembly and alignment approach for OVIRS is to align the elements in phases within each alignment step, where each phase progressively improves alignment to the limit of its capability [21]. Each phase is characterized by the units associated with the difference between the alignment state realized at the end of the phase and nominal, ambient alignment configuration. The plan starts with inputs to the component design to allow indirect access to the mirrors' optical surface via alignment fiducials and includes "calibration" of the fiducials by the vendor. The assembly work starts with coordinate system definition and a "rough alignment" phase for each component, where the elements are aligned using mechanical metrology to a fraction of a mm. The second, mid-range phase ends with elements aligned to microns and arcsec using optomechanical metrology techniques and alignment fiducials. The third, and final, phase ends with the system alignment optimized such that the wavefront error is measured in nm and is dominated by fabrication errors on the mirrors. The third phase may be simply a calibration of the wavefront error, if performance requirements are met (i.e., no active re-alignment may be necessary). This work describes the implementation of this plan, highlighting the steps that utilize optical metrology techniques for testing and alignment.

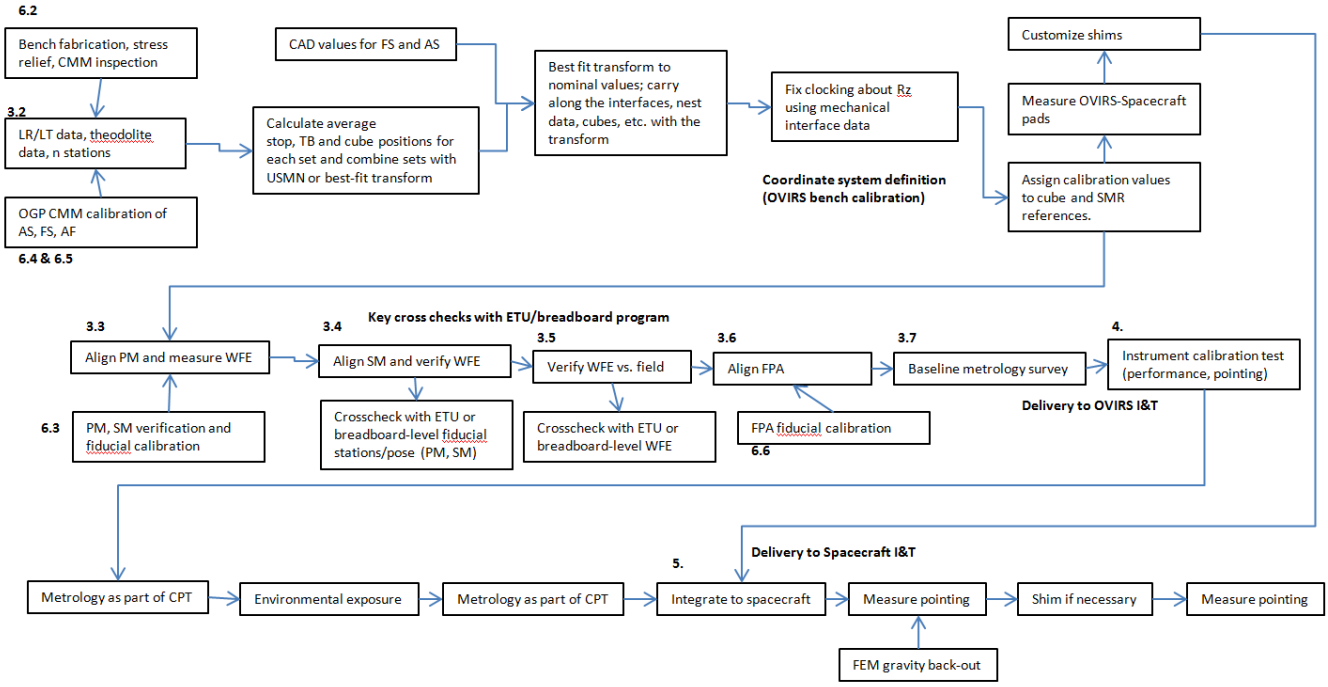

Figure 3-2. Process flow for OVIRS alignment plan.

3.2 FLIGHT MIRROR CHARACTERIZATION

The OAP's were diamond turned optics fabricated by Corning, Inc. [22]. Corning diamond turned the rear surface of the primary and secondary mirror to a flat prescription, such that the normal of the surface would parallel to the optical axis of the OAP.

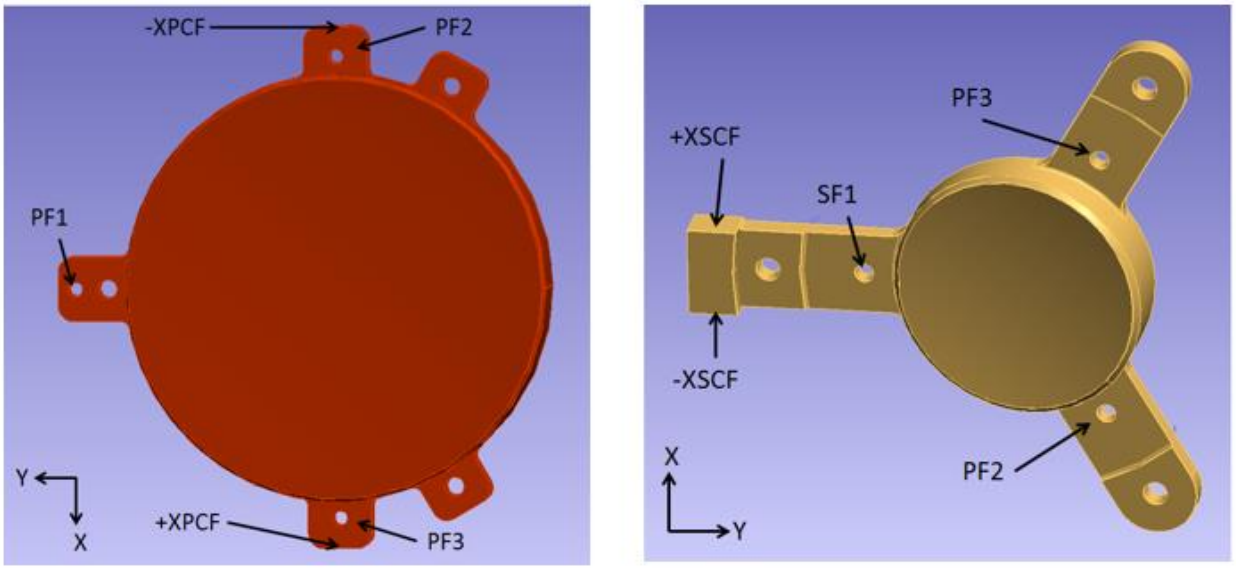

Figure 3-3. Primary and secondary mirror schematic of alignment fiducials.

The figure above illustrate the fiducial on the two OAP's. Each OAP had three holes fibricate onto the mirror in which the hole routine for the laser radar could be used charaterize their location with respect to the focus. Those fiducial holes are denoted in the figures as SF1, 2, and 3 and PF1, 2, and 3. The clocking fiducials for the OAP's use to track the in-plane rotation about the optical axis were diamond turned flats located on +/-X face of the mounting tabs for the primary (+/-XPCF) and the as well as the +/-X face and the longest mounting arm for the secondary. Together, this array of alignment fiducials provided references for all six degrees of freedom (DoF) for alignment of each mirror during integration.

The first step in the alignment process for OVIRS was to characterize each of the OAP's position of best focus with respect to the mirror fiducials. The characterization was completed using theodolites, the laser radar, and a VERIfire interferometer [23]. A theodolite was aligned to the collimated beam from the interferometer, setting the reference for the optical axis. The OAP where mounted in a three degree of freedom kinematic mount that allowed for the fine alignment of rotation about all three axes.

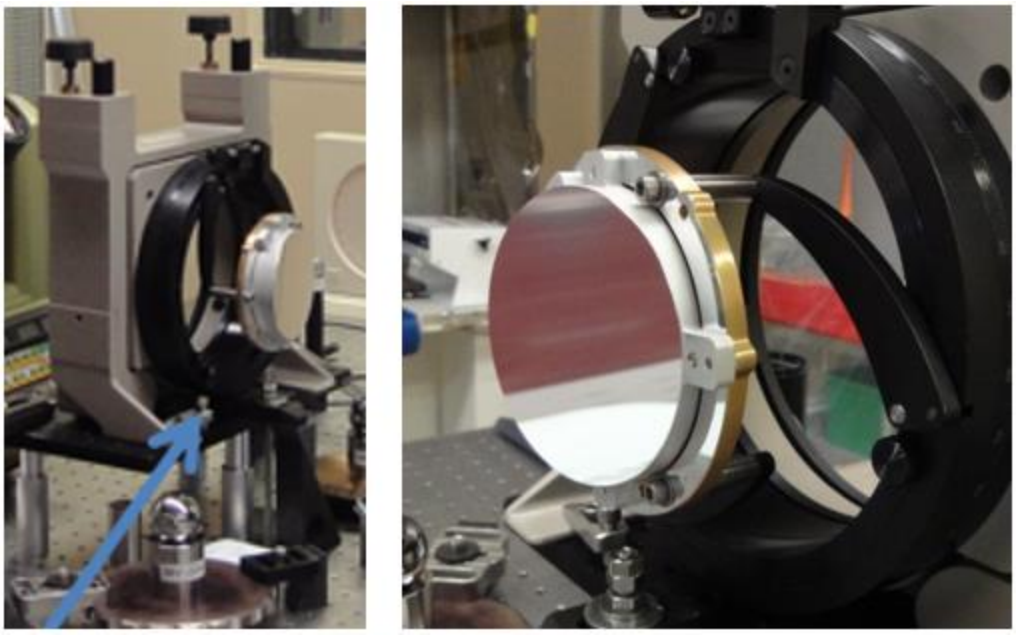

Figure 3-4. Primary mirror mounted on kinematic tip/tilt stage.

The OAP in the three degree of freedom mount was rough aligned to the interferometer in front of the theodolite to identify the interferometer axis. Using the fine adjustments on the mount the OAP was then align to the theodolite so that the optical axis of the OAP would be parallel to the axis of the interferometer. Using the hole routine on the laser radar to get in the OAP's coordinate frame, the laser radar was used to point to the focus location of the mirror. A ciliball was places at the focus location on combination of three linear stage that allowed for fine alignment in both planar axes and the piston direction.

The course alignment was achieved in this manner using the laser radar, after which the fine alignment to the Fizeau was obtained using the three DoF linear translation stage: A fringe pattern was captured for the initial, rough-aligned state. The phase-shifting algorithm of the commercial Fizeau interferometer was used to interpret the fringe pattern in terms of low-order, Seidel aberrations for this double-pass test. We then used the kinematic mount to rotate the OAP in tip and tilt in a systematic manner, moving the Caliball in field space accordingly to obtain a good null (i.e., low power and tip/tilt) and record wavefront error. We used this technique to minimize astigmatism and then coma. At the completion of this fine alignment stage, a baseline figure error map was recorded for the best alignment condition.

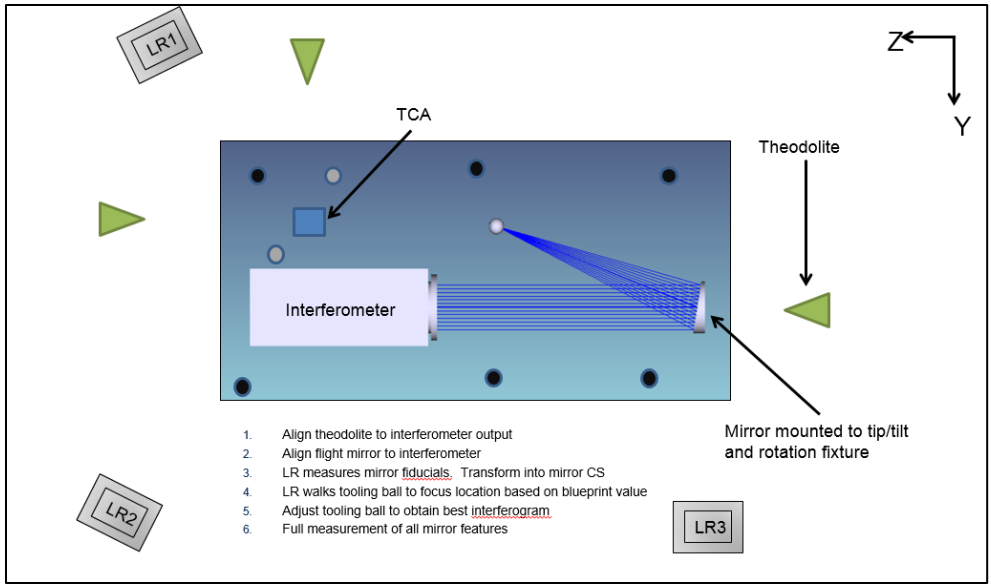

Figure 3-5. Schematic of mirror focus characterization.

Once the fine alignment of the OAP was obtained, we used the theodolite positioned on the back of the mirror in concert with the fine adjustment feature of the optical mount to interrogate along the vertical and horizontal axes to find the position of best focus. This process was completed for all four of the flight OAP's as well as the pathfinder primary and secondary OAP. Once that position of focus was recorded, a full characterization of the setup was performed. The metrology setup is illustrated in the figure above.

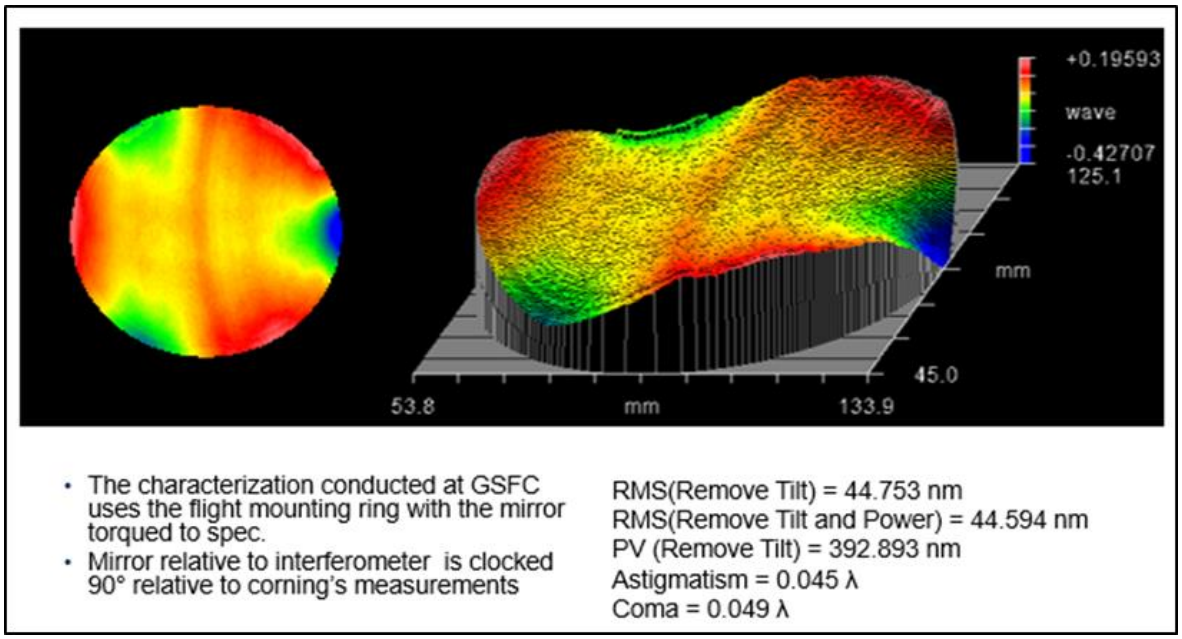

Figure 3-6. Surface figure map and RMS of the primary mirror in Metropro software.

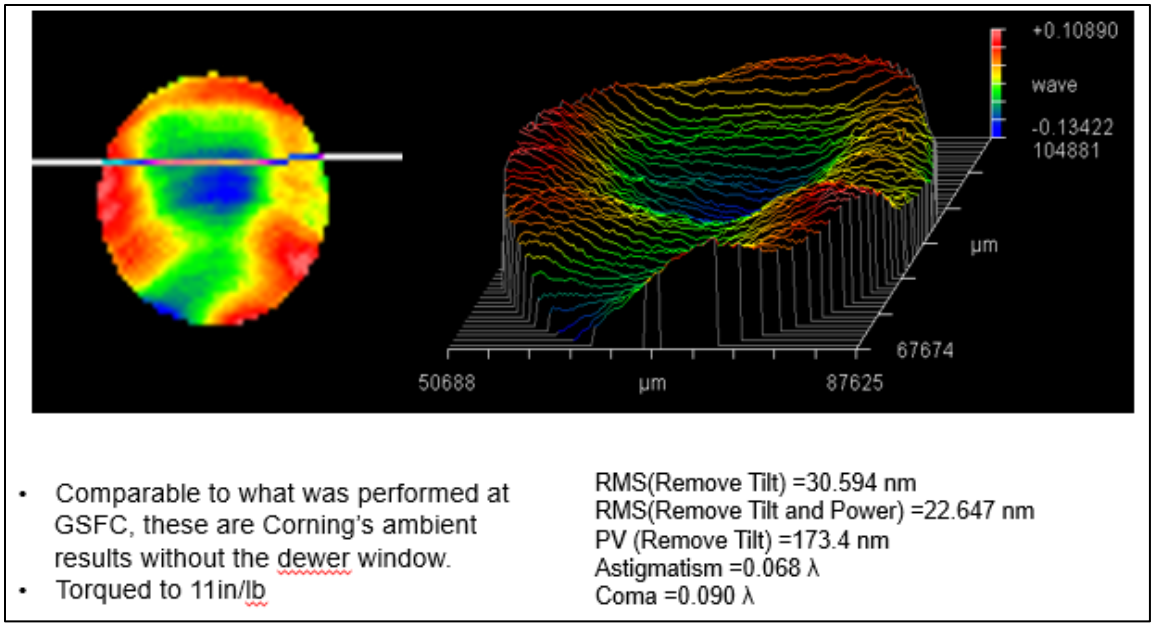

Figure 3-7. Surface figure map and RMS of the primary mirror in Metropro software.

The surface error on all four of the OAP's met the specification of 100 nm by a sizable margin. The primary OAP's had a surface error around 50 nm and the secondary OAP's had an error around 30 nm. We pick the primary and the secondary with the lower surface figure to be the flight mirror and the other two were the flight spares. The surface map from the interferograms of the two OAP's chosen for flight are below.

3.3 FLIGHT MIRROR MOUNTING ASSEMBLY

The OVIRS mirror mounts were the hardware interface between the mirror substrate and the OVIRS optical bench. The mounts were required to maintain mirror alignment through the rigors of launch (i.e., vibration and acoustic loading), while providing adjustability needed for the assembly and alignment process, while minimizing distortion of the optical surface. In addition, they were required to accommodate the significant temperature difference between the ambient, room temperature assembly environment and the flight environment. Errors in pose expected from the fabrication of the bench-mount interfaces and the mirror substrate-mount interface were accommodated by the mirror mounts.

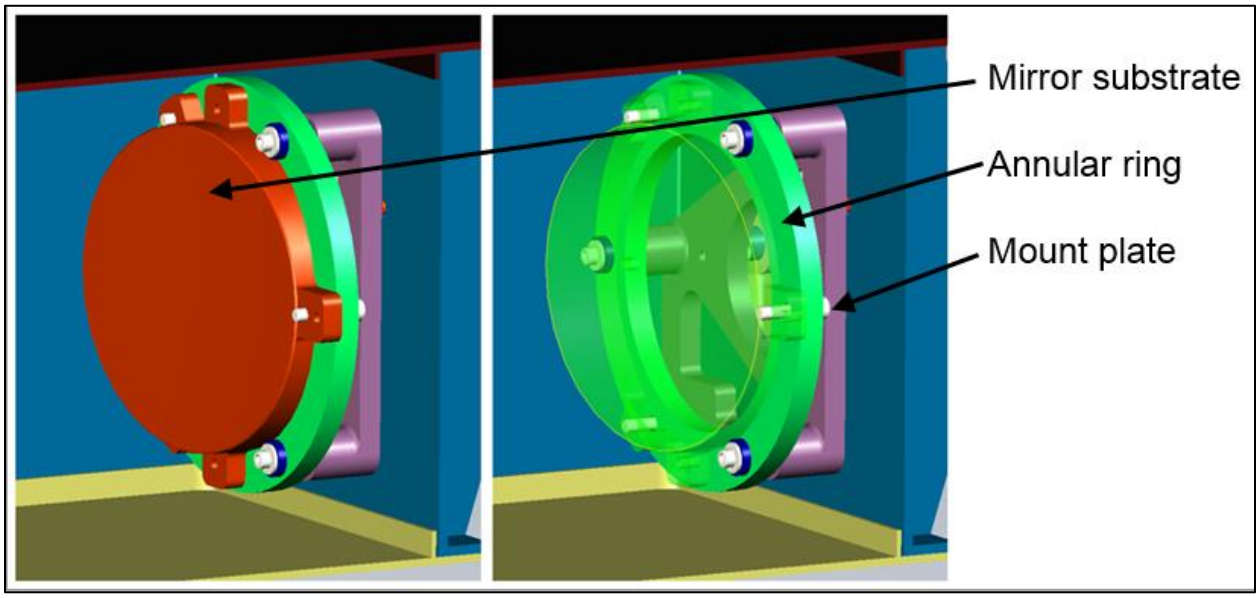

Figure 3-8. CAD model of primary mirror mounting assembly.

The initial design of the mounts is show in Figure x. The tabs on the mirror substrate provided locations for fasteners and interfaced to highly co-planar pads on an intermediate "ring." The tabs and ring helped isolate the mirror surface from stress associated with the fasteners and assembly process. The ring interfaced to a mount "block."

The component-level characterization and calibration of the flight mirrors was not conducted using the flight mounts, because the mounts were not fabricated in time and we needed an un-mounted baseline. For the component-level testing, we used a prototype of the primary and secondary OAP's rings to support the mirrors. When attaching the mirrors to their prototype rings, we were not able to use the flight torque value of 11inch-pounds without unacceptably distorting the mirrors. With lower torque settings, we obtained results that were

similar to the figure error values measured by Corning before delivery. This finding did not yet give us pause, because the flight ring design utilized spherical washer pairs intended to prevent mount-induced stresses in the OAPs.

When the flight interfaces for the OAPs were available, the OAP's surface figure was tested in a mounted configuration. In the figure below we show the hardware configuration for component level testing of the flight primary mirrors. As stated above, the mirror is attached the mounting ring and the mounting ring attaches to the mirror mount. The GSE is comprised of the stock that interfaces to the mirror mount. The stalk is hollow, allowing a theodolite to have line of sight to the back of the OAP. The stalk is held by a five DoF mount that is a combination of linear and tip/tilt mounts for fine alignment control.

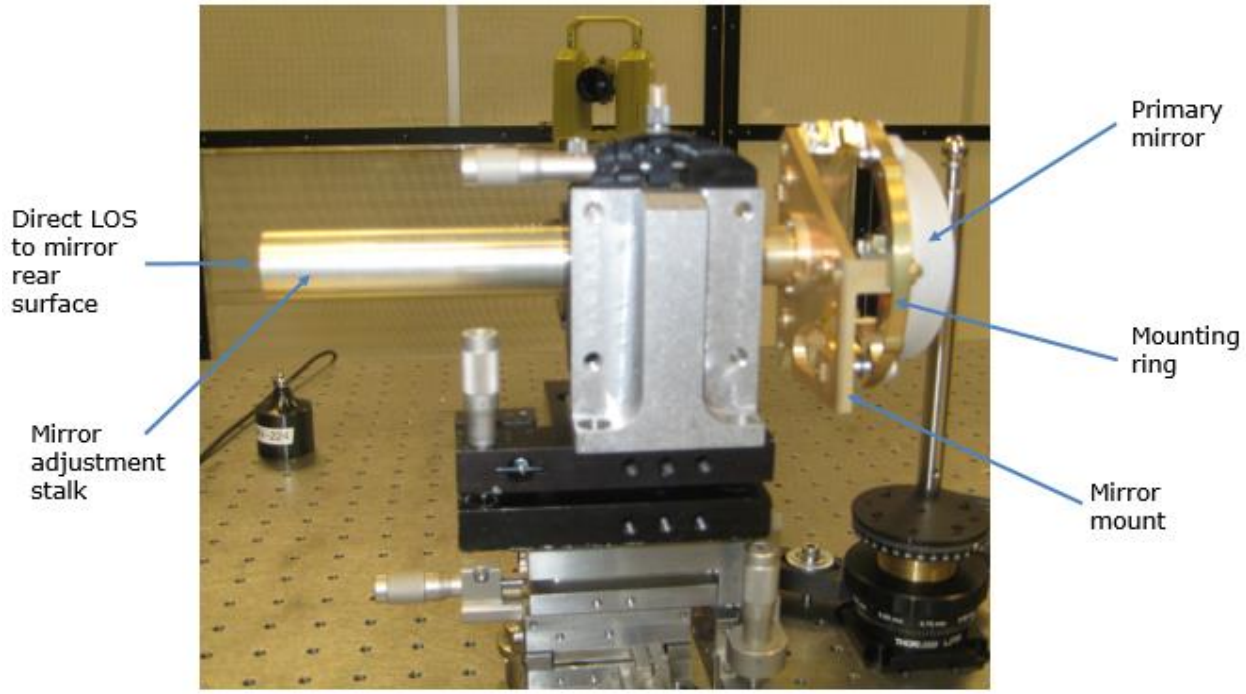

Figure 3-9. Kinematic opto-mechanical mount for mirror characterization and alignment.

The flight torque value of 11 inch-pounds was used in fastening the OAP to the flight mirror mount. After mounting the mirror, we performed a surface figure measurement to check whether the mounted mirror met the required surface specifications (with some additional, allowable degradation, as allocated in our error budget). We found that, when the mirror was fully torqued to the mount, the stress distorted the mirror, causing the surface figure error to greatly exceed its specification. Further trouble-shooting indicated that the spherical bearing

pairs did not provide the expected compensation for the stress in the ring-OAP interface. As a result, there were a series of re-design-and-test iterations for the mounting ring, attempting to address this issue.

Figure 3-10. Iterations of the interface ring for the primary mirror mount.

The original ring design is shown in the upper right of Figure x. The design was a solid, monolithic ring with the three mounting interfaces for the mirror using spherical bearing pairs between the ring and mirror. In the second design iteration of the mounting ring, the interfaces were diamond turned and the ring was light-weighted around the three mirror mounting interfaces to create flexures that would reduce stress in the mirror from mounting. This iteration improved the surface figure error of the OAP after mounting (i.e., it degraded less than for the original ring design). However, placing the primary mirror and ring sub-assembly into its flight mount was not repeatable and further degraded the figure error. While the primary mirror met the specification of <100 nm RMS with the ring attached, but, when the OAP+ring was removed from the stalk mount and returned, the mirror's RMS figure error further increased by ~50 nm and no longer met specification. This mount-then-test operation was repeated multiple times.

The attempts yielded figure error results that sometimes met and sometimes violated specification. This lack of repeatability lead to the next redesign.

The next iteration of the mounting ring is shown in the bottom figure in Figure 3-11. This ring had the same light-weighted design around the mounting interfaces to provide flexure to help relieve mounting stress. This ring had a triangular design to further mitigate deformation

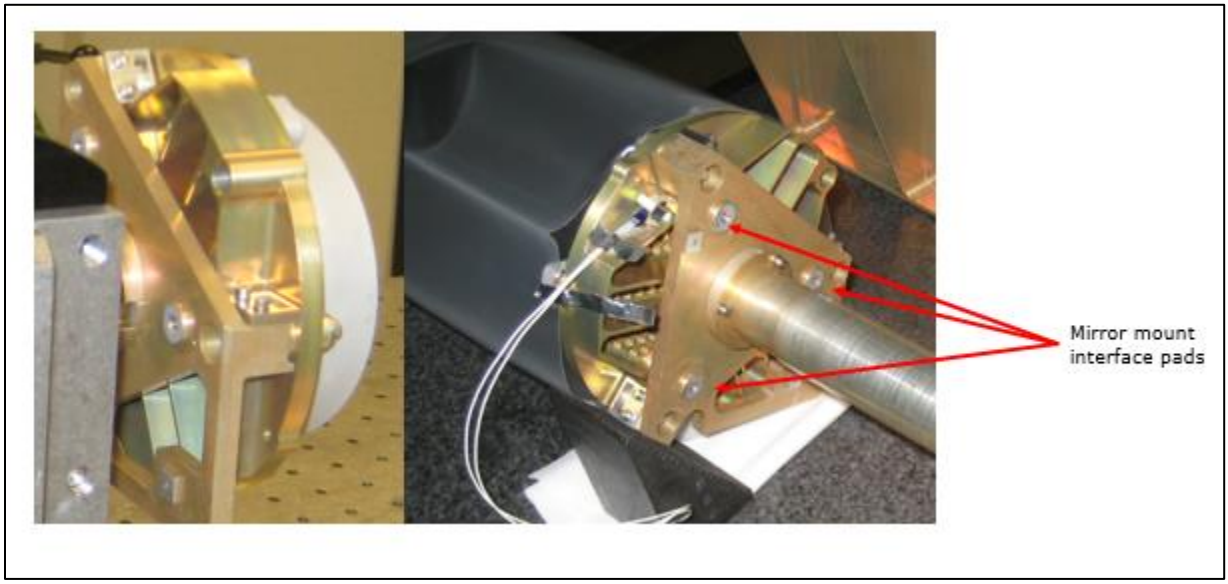

Figure 3-11. Final solid mount design for the primary mirror.

in the mirror. This third design iteration provided a better as-mounted surface figure than the previous two versions, but still suffered from poor repeatability that occasionally resulted in an out-of-specification figure error or met tolerance with very little margin.

The fourth and final iteration of the flight mount featured a solid, one-piece mount design instead of an intermediate ring+mount. Testing indicated that this solid mount provided surface figure that met specification and showed reasonable repeatability. The design was inspired by the mirror mount design from a previous NASA instrument, the Infrared Multiple Object Spectrometer [24]. Once it was determined that the mounting assembly for the primary mirror was deemed suitable, the interface pads on the bench-side of the mount were scanned with the LR and the position of the best focus for the OAP was re-characterized with respect to this interface. The scans of the interface pads were used in conjunction with prior scans of the interfaces on the optical bench to create a shim prescription. The final OAP-mount-shim-bench assembly utilized these customized shims to place the OAP's focus at the nominal focus location in the bench coordinate system to within our tolerance.

The design of the mounting assembly for the secondary mirror was not improved: No work was done to redesign the mount, despite an unfavorable initial measurement of the surface figure. We conducted a tolerance analysis using the optical model, which determined that the requirement on figure error could be relaxed to bracket it's as-mounted figure error and any non-repeatability. This updated analysis relied on the fact that the diameter of the footprint of the beam on the secondary mirror was significantly smaller than the clear aperture of the OAP. When the interferogram was masked-down to the diameter of the collimated beam, the surface figure error was acceptable.

3.4 OPTICAL BENCH CHARACTERIZATION AND COORDINATE SYSTEM DEFINITION

Upon completion of the primary and secondary mirror characterization, the installation of the optical component to the optical bench began. The "Obox" is both the light-tight housing for OVIRS and the bench that meters the path between the components. The mechanical coordinate system is defined by the nominal, CAD x,y,z values associated with the Obox-spacecraft interface. The coordinate system is referenced to three tooling ball locations on the top (i.e., -X side) of the box denoted by OB1-3. The instrument pointing and the rotations of the Obox are also referenced by the two optical cubes, OC1 and OC2. The Obox and the metrology target locations are illustated in Figure 3-12. The openings in the Obox behind the primary and and secondary mirror locations allow line-of-sight to the back of the mirrors for metrology purposes.

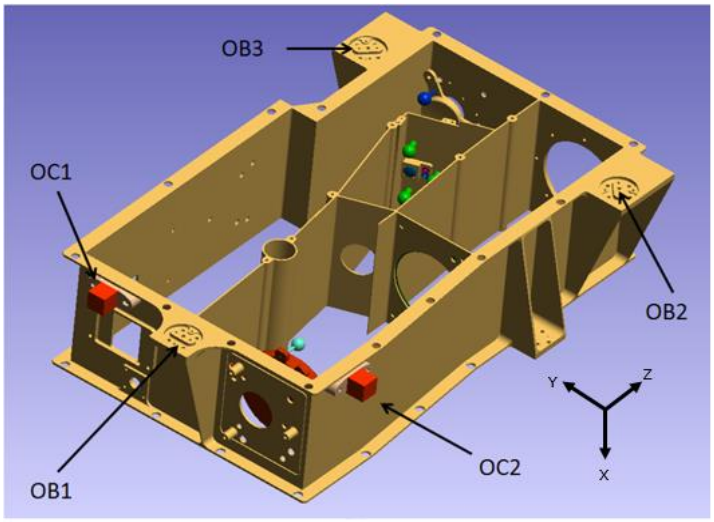

Figure 3-12. Obox and alignment fiducials.

Before system-level alignment, the instrument's coordinate system had to be established on the Obox. In attempt to use the interferometer pointing to set the systems optical axis, the Obox was aligned such that the output of the interferometer to be perpendicular to the gravity vector to an accuracy of ~<30 arcsec using an autocollimating theodolite that was leveled to gravity and focused on infinity. Next, the Obox was leveled to the interferometer, such that the interferometer's optical output essentially propagated parallel to the z-axis. The interferometer axis thus defined the optical axis and this pointing direction was referenced to the -Z face of OC1 via autocollimating theodolite metrology. Figure 3-13 is a picture of the Obox aligned in front of the interferometer.

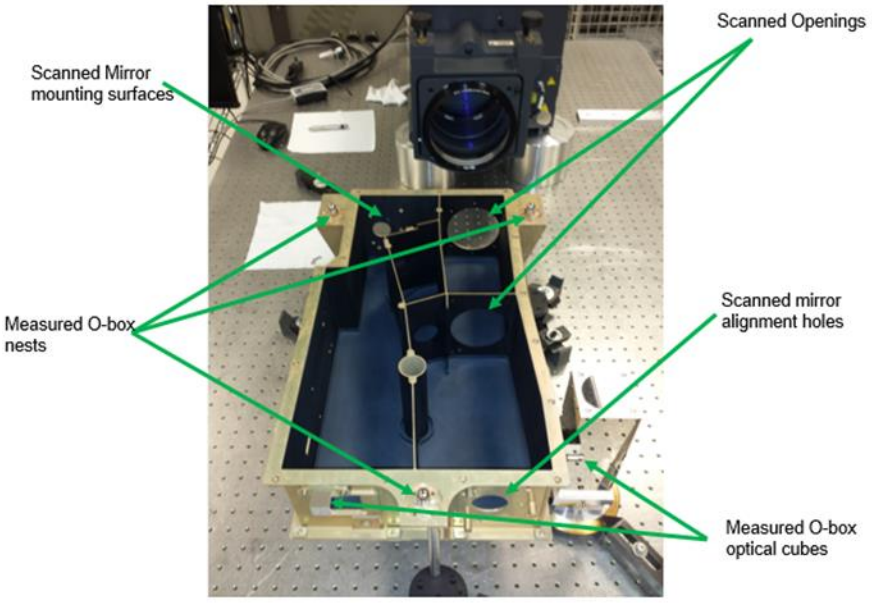

Figure 3-13. Test configuration for the Obox.

The optical cube measurement and the tooling ball locations were tie together via a separate Transfer Cube Assembly (TCA). This allowed the LR and theodolite to check for one another in characterizing the rigid body rotations of the system. The aperture opening as well as the mounting interfaces were scanned by the LR to ensure proper clearance for the collimated beam entering the system (i.e., to avoid vignetting) and to provide information for nominal shim prescriptions to be used in mating the primary and secondary mirror to the Obox, as mentioned in the previous section.

3.5 FIELD STOP CALIBRATION

The primary mirror fiducials where located nominally in the Obox coordinate system. The location of the primary mirror focus sets the location of the field stop in the optical system. Therefore, to determine where the field stop opening was located, the primary mirror characterization was transformed into the Obox coordinate system via the three mirror fiducials. Once the placement of the field stop was determine, a surrogate field stop was necessary for the purpose of verifying the alignment of the primary mirror once it was installed into the system and staked into position. Figure 3-14 shows the alignment process of the flight and the surrogate field stops. Also, notice that the flight field stop has a pertruded opening that insert into the Obox.

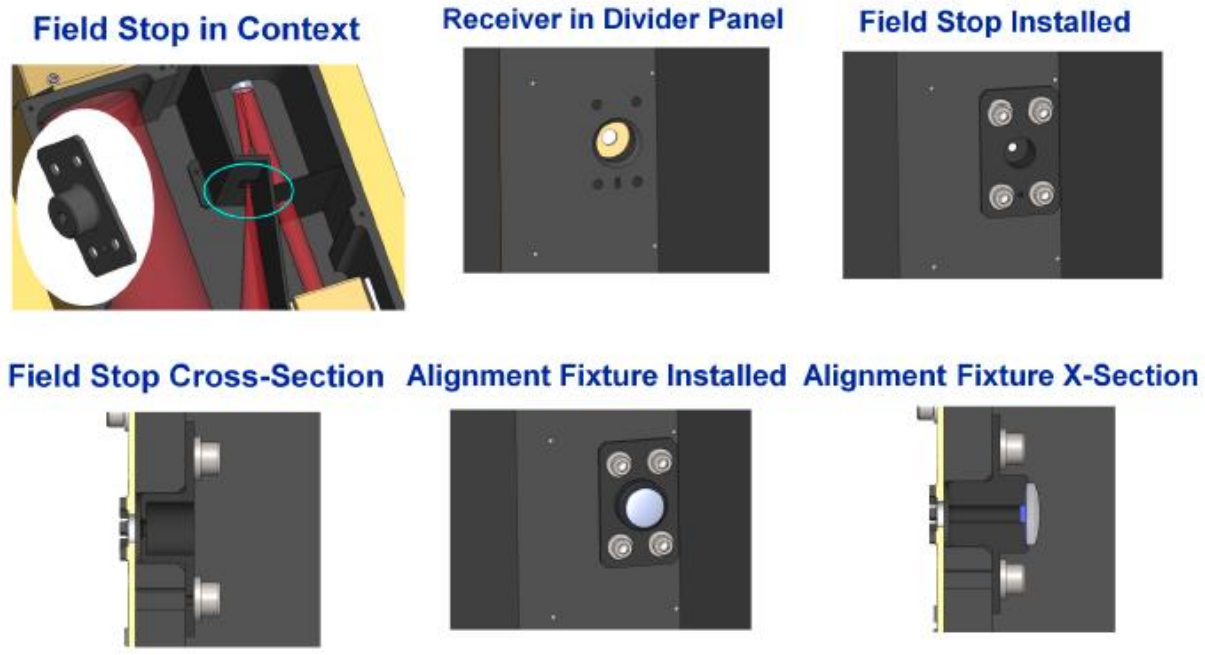

Figure 3-14. Schematic of the field stop in the Obox.

3.5.1 Surrogate Field Stop

The surrogate field stop consists of a coated lens whose center of curvature is measured using a LR via tooling ball function and three metrology nests that are measured and related to the lens center of curvature. After calibration, the surrogate is mounted into the Obox and the nests are measured with respect to the Obox nest to determine the lens center location in the Obox. The LR measurement of the spherical lens on the surrogate will be placed in SA ~350µm

behind the opening for the flight field stop. The image on the left in Figure x shows the surrogate and the figure on the right is an illustration of how the spherical lens relates to the field stop opening. This GSE surrogate field stop was used to verify the alignment of the flight field stop as well as align the primary mirror before the final installation of the flight field stop.

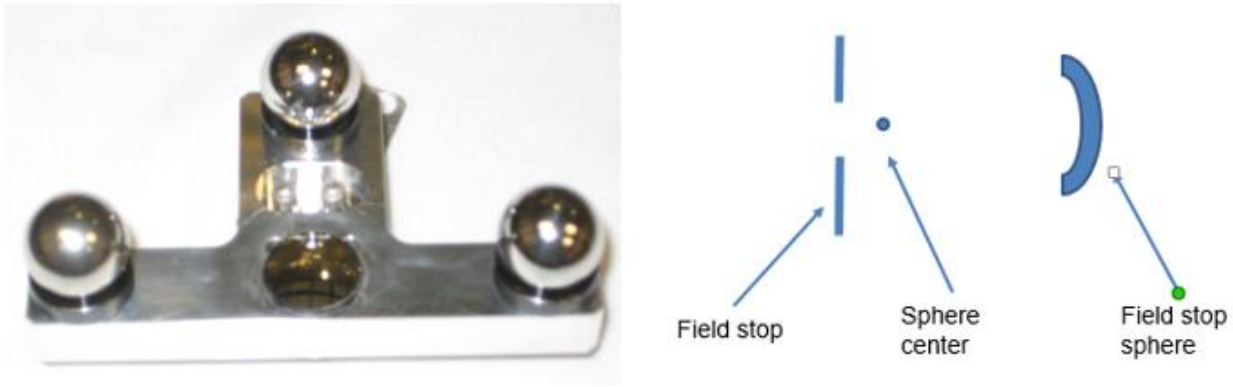

Figure 3-15. Surrogate field stop.

3.5.2 Flight Field Stop

Separate from the surrogate field stop calibration, we installed and measured the flight field stop. When the flight field stop was installed into the Obox using nominal shims, the Obox was characterized in that configuration using the LR and theodolites. The opening of the field stop was scanned with the LR, as a check, and related to the Obox coordinate system by measuring the three Obox nests. At that point, the result of the characterization of the flight field stop configuration and the surrogate were combined into one file in SA and the two data sets were best-fit via the Obox nest targets. The distance between the position of the spherical lens center and the plane of the flight field stop opening was obtained. We expected the surrogate and flight field stops to be aligned to the same location, to within small measurement and assembly error. However, the nominal placement of surrogate proved to be incorrect (i.e., there was an error in the shim prescription), and shims to correct the placement of the surrogate were added. The surrogate field stop in the Obox characterization was repeated, showing good agreement

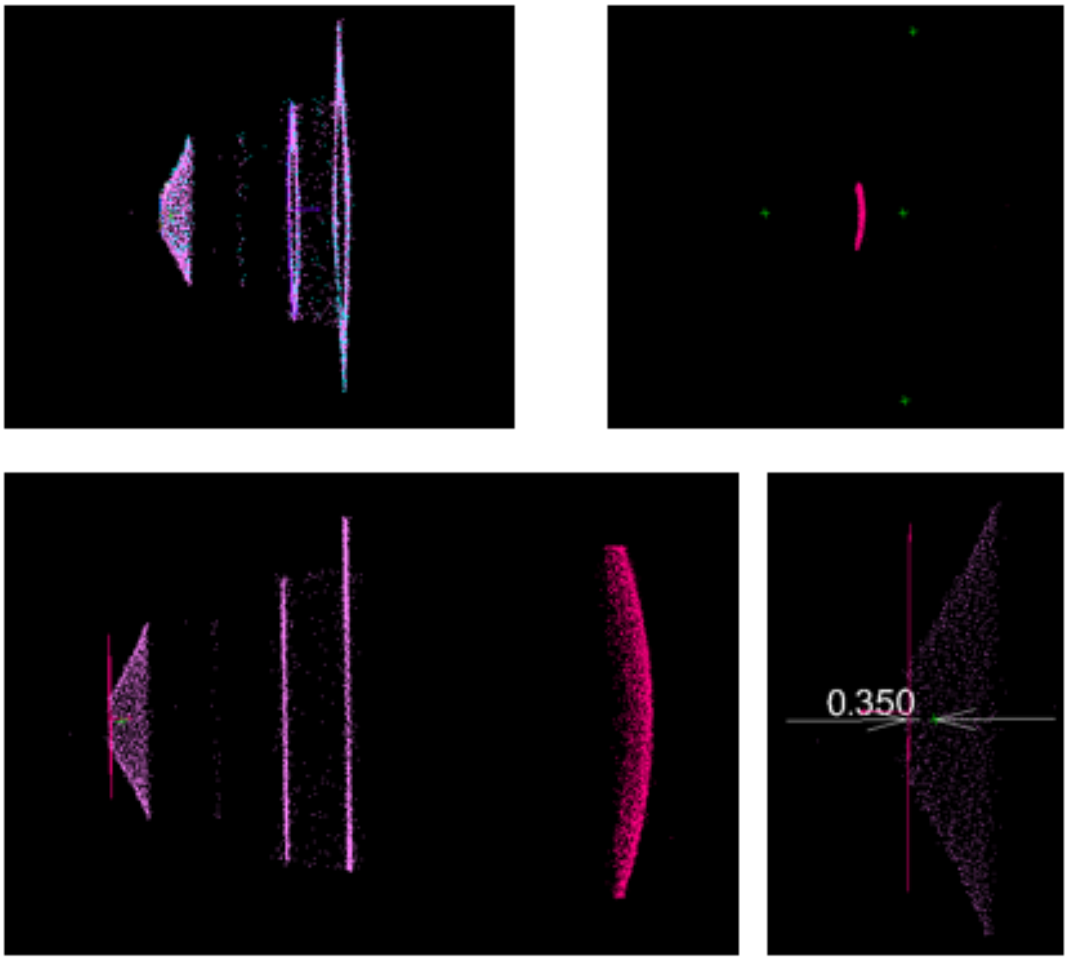

Figure 3-16. Spatial Analyzer analysis of laser radar metrology on the field stop.

The results of the field stop characterization in SA are illustrated above in Figure 3-16. The figure in the top left corner shows the scans of the flight field stop. The scan is of the inside of the stop and the end of the beveled opening is the opening is the aperture. The figure on the top right is a scan of the spherical lens and the points on the surrogate field stop. The bottom right is combination of the scans of the field stop and the surrogate to show the location of the spherical lens center in comparison to the field stop opening. The bottom right image is a close up of the lens center and the field stop open with the dimension to show that the surrogate field stop is installed in the correct position.

3.6 MIRROR INSTALLATION

Upon the completion of the component level testing of the flight optics, verification of the field stop location, and the characterization of the Obox, the installation of the flight hardware to the Obox began. The first step in the integration flow was to install the primary mirror.

3.6.1 Primary Mirror

The primary mirror and surrogate FS installed to O-box nominally with the shims prescription obtained from the scans of the primary mirror mounting assembly's mounting interface scans. In principal, the normal of the back surface of the primary mirror was parallel to the Z-axis (optical axis) of the system. The O-box was aligned to the interferometer by using a theodolite to walk in the primary mirror rear surface to the interferometer beam.

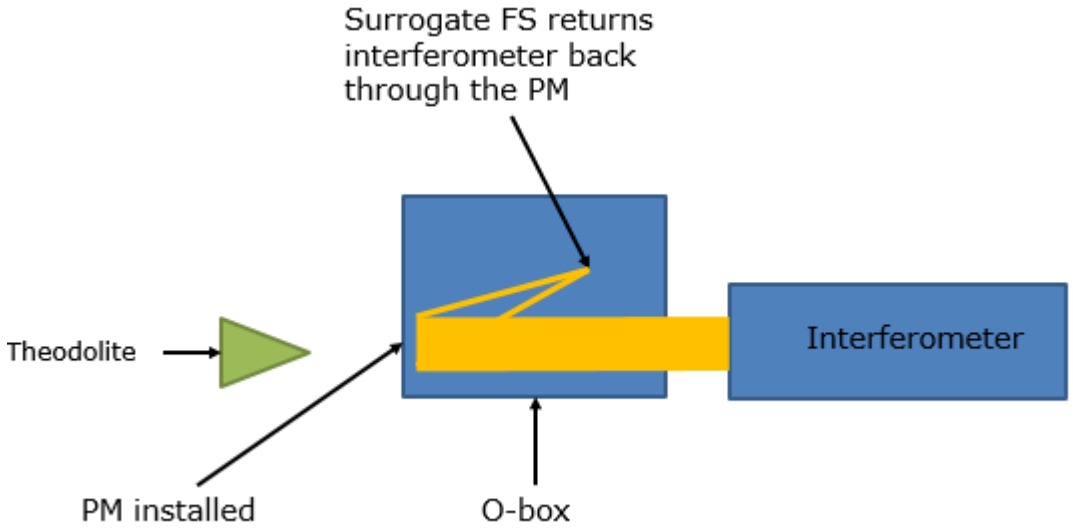

Figure 3-17. Primary mirror installation test setup.

The Interferometric measurements of the primary mirror figure error in this setup for the nominal primary mirror placement in the Obox resulted in non-zero power --- i.e., the OAP was initially out of focus. The primary was removed and re-installed with the shims calculated from the characterization of the flight mirror assembly, as mentioned above. This reduced the power, but the wavefront still did not reflect zero power. There was also a slight misalignment in the X-Y plane resulting in a slightly higher surface wavefront error for other low-order terms than what was achieved at the component level testing for the primary.

The nominal bushings were removed and attempts were made to adjust the mirror in the XY plane. This proved to be very difficult. Stages were used to position the mirror, but, when torqued, the mirror quickly misaligned. The misalignment during the torqueing phase was not predictable and varied. The GSE for adjusting the box was not stable enough to hold the O-box in place while adjusting the primary mirror. The solution was to insert the nominal bushings for the final mounting to the O-box and correct the wavefront error by slightly altering the instrument pointing with respect to the interferometer --- i.e., we effectively changed the coordinate system (or instrument boresight calibration) to reduce the coma and astigmatism in the primary mirror, but not enough to induce vignetting of the beam by the Obox hardware. Once the wave front compared more favorably to the component-level results, the final pointing with respect to the interferometer was recorded and a brief study was conducted to insure that the alteration in the instrument pointing would not cause issue with the system level requirement of the instrument pointing and vignetting. It was determined that instrument was still within the 10 μradian specification of the pointing relative to the nominal optomechanical axis.

3.6.2 Secondary Mirror

The next step of the integration process was the installation of the secondary mirror into the Obox. Since the adjustability of the primary mirror was found to be difficult the nominal bushings were installed with the shims determined by scanning the mounting interfaces. At this point the surrogate field stop was replaced with the flight field stop and the secondary mirror was installed nominally with the shim prescription. A large flat mirror was placed in the setup such that it could partially be measured by the interferometer and covers the output of the OVIRS instrument. The Obox was aligned to the interferometer via the rear surface of the primary mirror based on the relation to OC1 obtained from the pointing direction in the installation of the primary mirror. The flat mirror was aligned angularly to the interferometer such that the minimum tilt was obtained in the wave front. The wave front was measure via a double pass interferometer test as illustrated in the figure below. The O-box was then tipped and tilted until the interferogram was nulled and the tilt coefficient was minimized the tip tilt was found to be within an arcminute of the rear mirror surface normal.

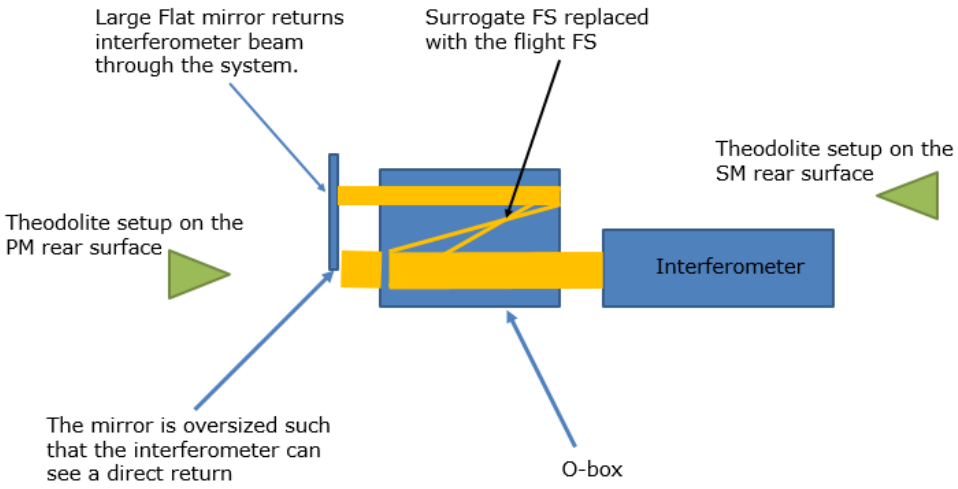

Figure 3-18. Secondary mirror installation schematic.

This configuration became the baseline for the integrated Obox collimated beam setup with the primary and the secondary mirror. Metrology was performed of this configuration to characterize the Obox nests, pointing of the rear surface of the primary and secondary mirror, pointing of the flat mirror, pointing of the Obox optical cubes, and the pointing directions of the clocking fiducials on the primary and secondary mirror. The instrument pointing still met the 10μradian requirement for the optical axis and the wave front was within the specification. The figure below shows the system wave front error.

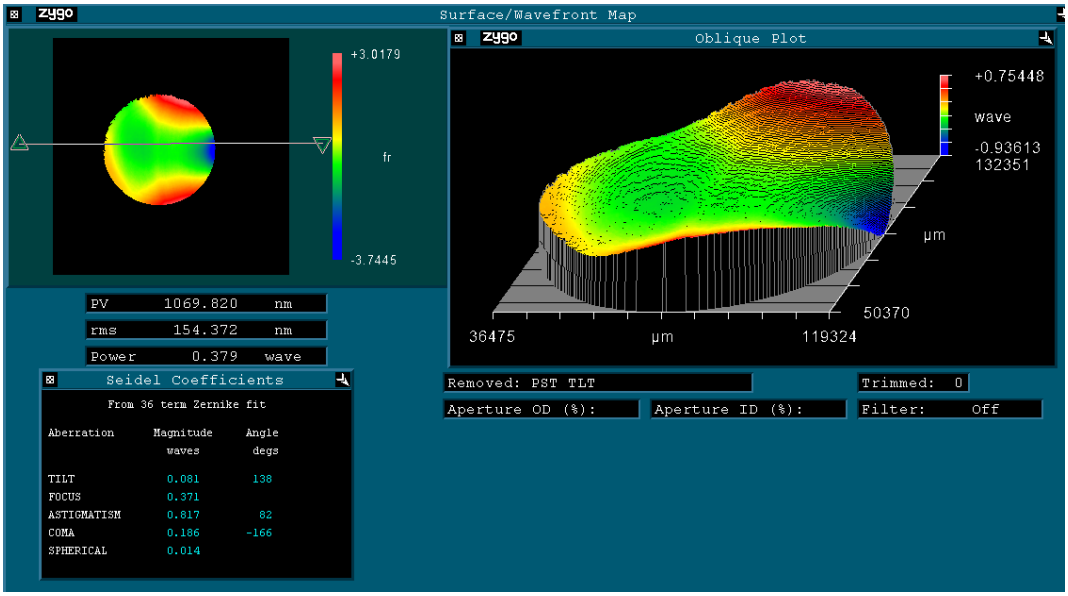

Figure 3-19. System wavefront surface map from Metropro software.

3.7 VIGNETTING (FOV) TEST

The field of view requirement for the spectrometer was 4 mrad. In order to check the instruments field of view, the Obox was place in front of the interferometer at the position of minimum wavefront error. The interferometer was the switched into it alignment mode, providing a more intense beam. A piece of paper was the placed in the bean path such that we could see the collimated beam spot. The azimuth and elevation of the back of the primary mirror were recorded and the position was considered the center point for the vignetting test. The O-box was tipped and tilted in each direction (up, down and side to side) until the beam disappeared on the paper. the theodolite was aligned to the primary mirror rear surface to monitor the angular position at each extreme. The theodolite values were recorded in each direction at the point in which the beam started to clip and when it fully disappeared.

Table 3-1. Vignetting Test Results

	Units: mrad		
	Start cutoff	Mid	Beam gone
El total range	3.66	3.81	3.97
Up from nominal	2.09	2.15	2.22
Down from nominal	1.57	1.66	1.75
Az total range	3.51	4.03	4.55
Left from nominal	1.62	1.85	2.08
Right from nominal	1.89	2.18	2.46

The table above list the results from the vignetting test. The number in the column up/down and left/right from nominal are the distance in mrad from the central beam spot. The total FOV in the elevation and azimuth directions are stated in the total EL and total Az rows. The test prove that the instrument met the FOV requirement of 4 mrad.

3.8 DETECTOR

The final step in the integration flow before OVIRS was closed up and went into cryogenic testing was the integration of the OVIRS detector. As stated earlier, the detector assembly has linear variable filter (LVF) design that sit inside of a housing which integrates to the Obox. The detector mask and the detector housing had to be calibrated separately using the Micro-Vu for the detector mask and the LR for the housing.

3.8.1 Detector Mask and Housing

The Micro-Vu proved to be the most accurate source for characterizing the detector mask opening to provide the footprint of the detector aperture. The purpose of characterizing the detector mask was to relate the edges of the detector to the tooling ball locations attached to the detector housing, DH1 and DH1B, as well as the plane of the front face of the detector housing. The front plate of the detector housing was attached to the detector mask, therefore all the targets on the detector housing were not available during the Micro-Vu measurements. The figure below is the Micro-Vu measurement of the detector mask in SA.

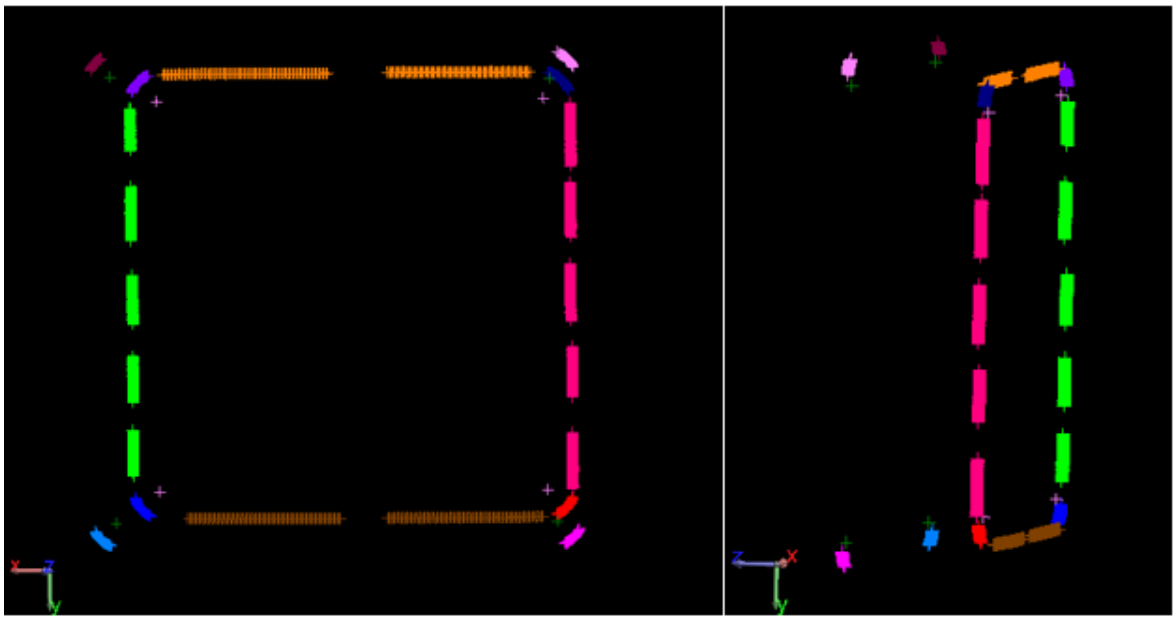

Figure 3-20. Micro-Vu measurement of the detector displayed graphically in SA™.

A second characterization of the fully assemble detector housing was completed. This characterization was for the purpose of relating DH1 and DH1B to the other two targets, DH2 and DH3 as well as a metrology scan of the plane of the detector housing's front plate. In the Micro-Vu measurements, only two of the four tooling ball locations could be measured in the configuration, DH1 and DH1B, because those were the only two targets on the detector housings

front plate. This presented an issue because three targets are needed to for a best-fit transformation. The normal vector of the plane of the front plate was used to lock down the last degree of freedom. A coordinate frame was created in both SA files using DH1 as the origin, the +Y axis defined by the line running from DH1 to DH1B, and the +Z axis was define by the normal to the plane of the detector front plate.

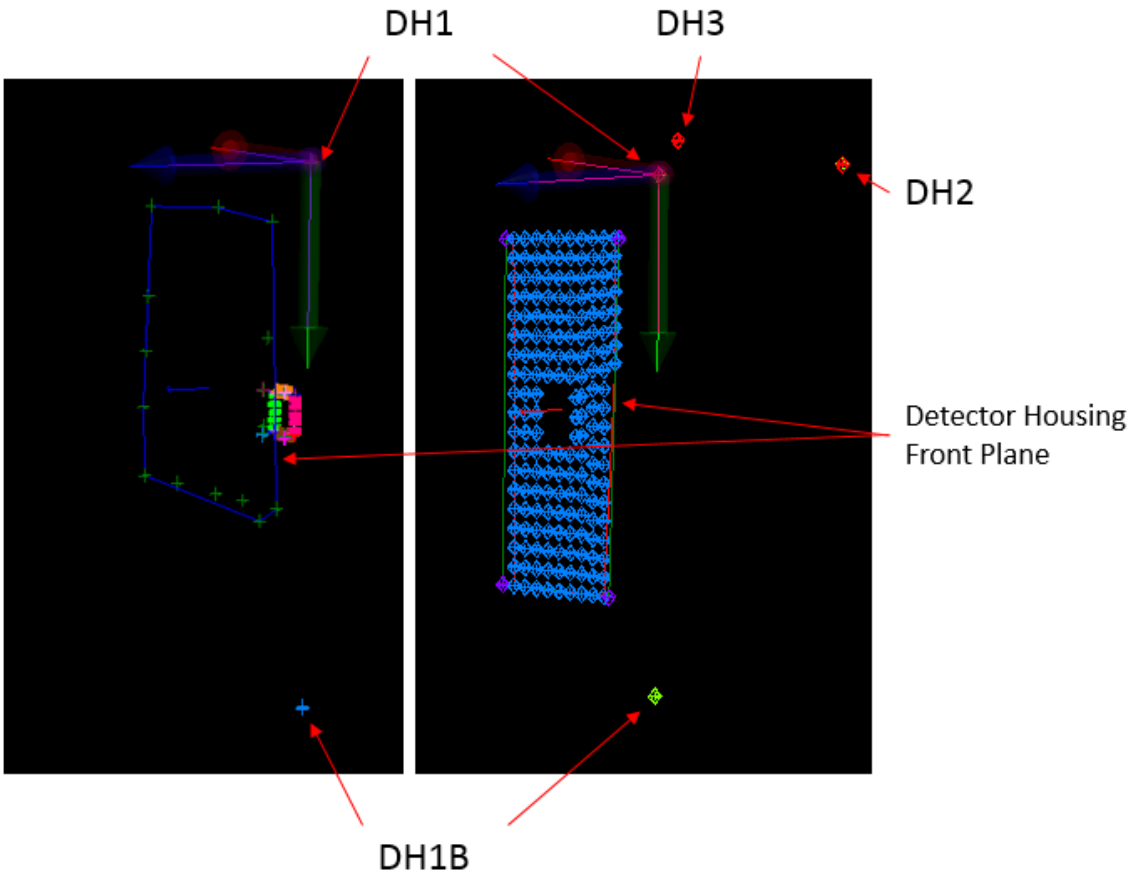

Figure 3-21. Detector characterization transformed the Obox frame displayed graphically in SA™.

The figure on the left is the Micro-Vu measurement of the front plate plane of the detector housing, DH1 and DH1B, the detector mask, and the detector frame. The illustration on the left is the LR characterization of the detector housing. The detector mask was not measured, but the mask opening can be seen from the scan of the front plate.

3.8.2 Beam Characterization

In an effort to align the detector in the Obox thus the detector was completely saturated, and idea for characterizing the collimated beam was developed. The tracking function of the

laser tracker in conjunction with the interferometer provided the ability to map the collimated beam diameter at multiple plane along the shot line. The LT was first tied into the coordinate system via the three Obox nest. Once the LT was in the coordinate system a plane at the nominal location of the detector was created in the SA file. Two more plane were created as well at another point inside of the box and one outside of the Obox.

Using the tracking function of the LT, a watch window was place on the plane so that an SMR could be walked into place. An SMR was place a stage that allowed for translation in along the X, Y, and Z-axis. The SMR was turned towards the interferometer such that a return could be seen in the Metropro software. Once the SMR was walked into the plane according to the watch window, the SMR was then move to the edge of the beam. The operator could see the edge of the beam based on the interferometer return. The return would compress before disappearing, indicating that the SMR was no longer in the collimated beam. At the point the SMR was turned away from the interferometer and towards the LT. That point in space was then measured by the LT.

That process of rotating the SMR toward the interferometer and moving to the edge of the collimated beam was repeated until roughly eight points were recorded around the radius of the beam. The method worked very well. The figure below shows the eight points taken around the radius of the circle and the circle constructed from the point in SA on the left. The illustration on the right shows the check of the collimated beam. That process of recording points along the radius of the beam was repeated at multiple plane, one inside the box and one outside of the box. The radius of the multiple circle were compared and a cylinder was constructed from the multiple beam circle to illustrate the collimated beam.

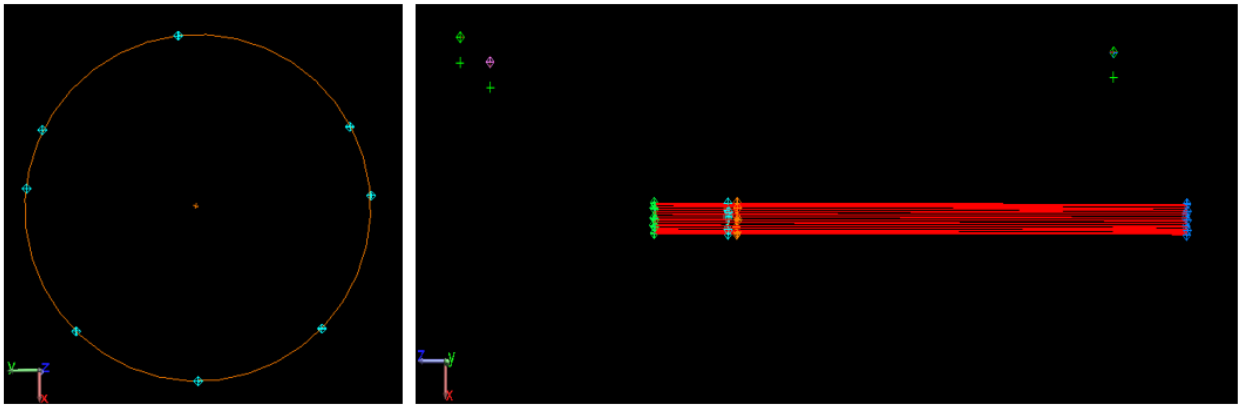

Figure 3-22. Illustration of the collimated beam in SA™.

3.8.3 Nominal Location

The detector housing was installed nominally into the Obox after first completing a vision scan of the side wall of the Obox at the location of the mounting interfaces. Upon installation of the detector, a laser tracker was used to measure the detector nests with respect to the Obox nest targets. The results were analyzed in SA and then the detector characterization and the beam characterization were combined into the file by best-fit transformation via the Obox nest targets. The beam location was then compared to the detector mask opening.

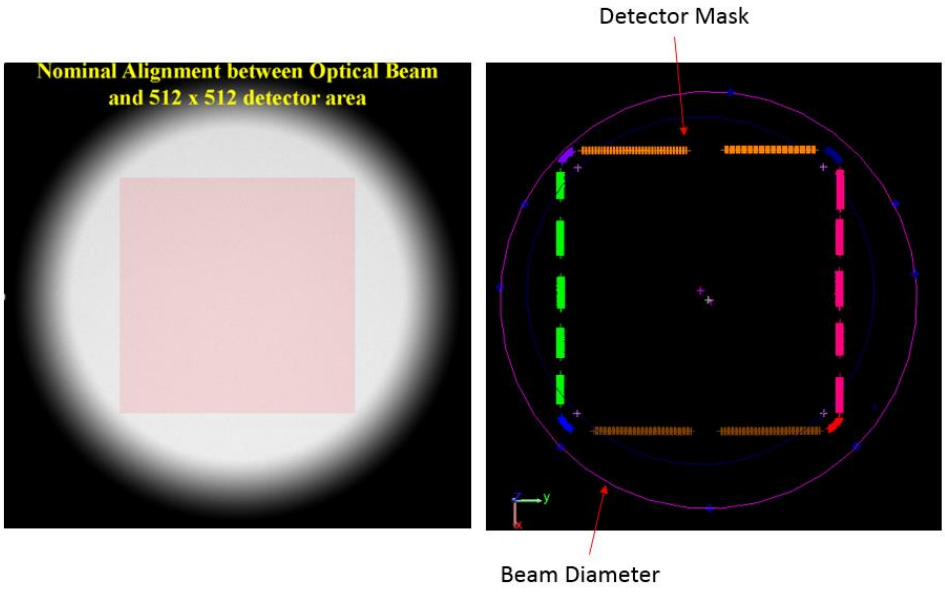

Figure 3-23. SA™ depiction of the detector position with respect to the collimated beam.

The image on the left is an illustration of the beam should overfill the footprint of the detector. The illustration on the right is from SA. The outer circle is the beam of collimated beam in the Obox while the square is the Micro-Vu measurements of the detector mask. The

detector does fit into the beam with the nominal installation of the detector, however the top left corner of the detector is just inside of the beam, therefore shims were calculated in the Y direction (from the detector mounting wall of the O-box). The detector was reinstalled with the cut shim and the detector was adjusted using the LT watch function until the X alignment was desirable. The detector housing was then pinned to the box and another set of measurements were made of the tooling ball nests in order to confirm the final location of the detector mask.

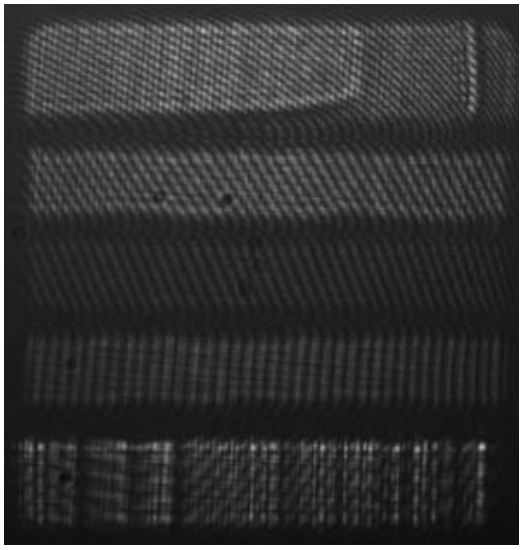

Figure 3-24. Interferometer return from LVF.

After the detector was pinned, the Obox was then place in front of the interferometer to check the alignment of the detector as shown in Figure 3-24. There was no requirement of a wavefront because of the detector LVF design. Each of the five strips in the LVF produce its own fringe pattern, therefore interferometry can't serve as a metric on the system align. However, a fringe pattern was produced therefore, by measuring OC1 and OB1-3 the position of the Obox with respect to the interferometer was used as one of the system test to verify that the internal element of the instrument did not move during environmental testing.

3.9 THEODOLITE SYSTEM THROUGHPUT TEST

To check the pointing of the system, we used a LT in conjunction with a theodolite and two SMR's to verify the boresitght of the as-built OVIRS instruments. The process began with building a reference file in SA™ using the ray trace model of the system best to the as-built Obox nest value. From this model, a line could be constructed along the chief ray of the instrument. On this line, two points were created outside of the Obox two be used as reference values to set up the theodolite.

The setup for the boresight test can be seen below in Figure 3-25. First the Obox nest were populated with SMR's for the LT. We measured the three Obox nest targets in order to best-fit the LT into the coordinate frame of the reference file with the two points along the chief ray. Once the LT was in the coordinate frame, an SMR was place onto two separate post that were attached to 3 DoF linear translation stages allowing for fine alignment in the two transverse axes and the piston direction. Using the tracking function of the LT, a watch window was created for each point and the two SMR's were walked into position. At this point in time the SMR's were replaced with dot targets (size of half in. tooling balls with a dot in the middle of a "bull's eye" at the center).

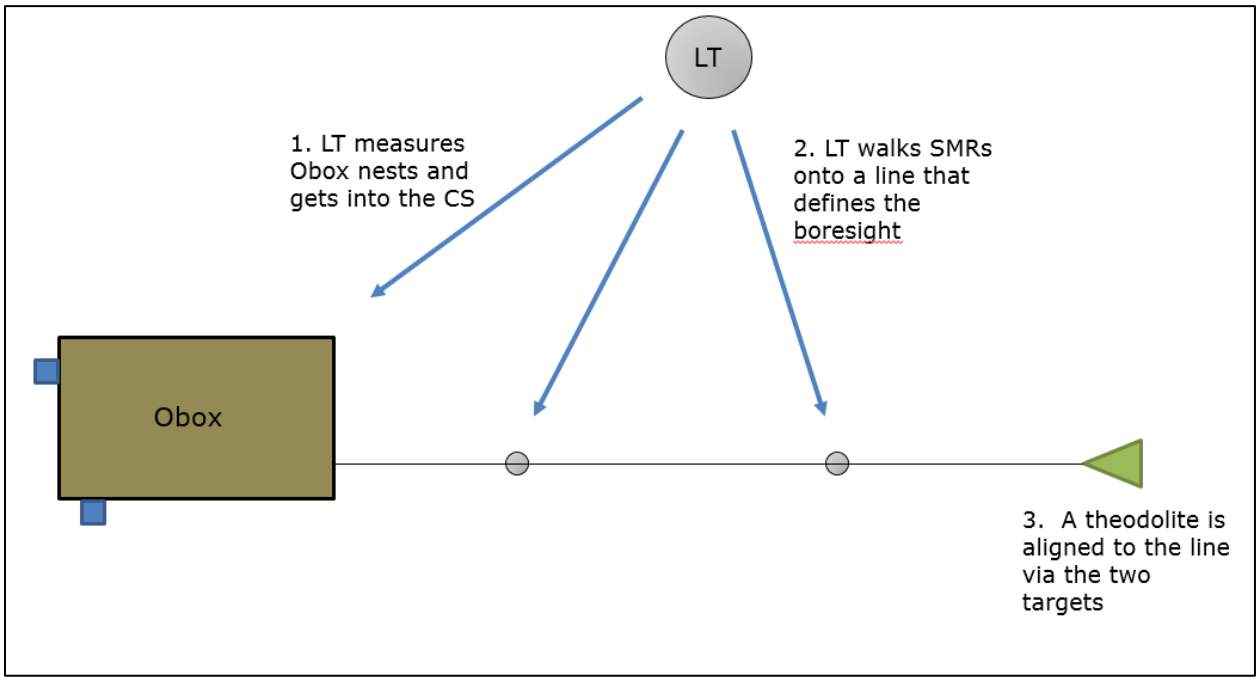

Figure 3-25. Test setup for the theodolite system throughput test.

A theodolite was rough place in line with the dot references. We were then able to use the dot references to align the theodolite along the chief ray. This process was an iterative

process that involved aligning the theodolite such that the dot on the target would fall on the center of the theodolite crosshair for the first dot. Then once the first dot was remove the theodolite crosshair would line up on the second dot without any adjustments.

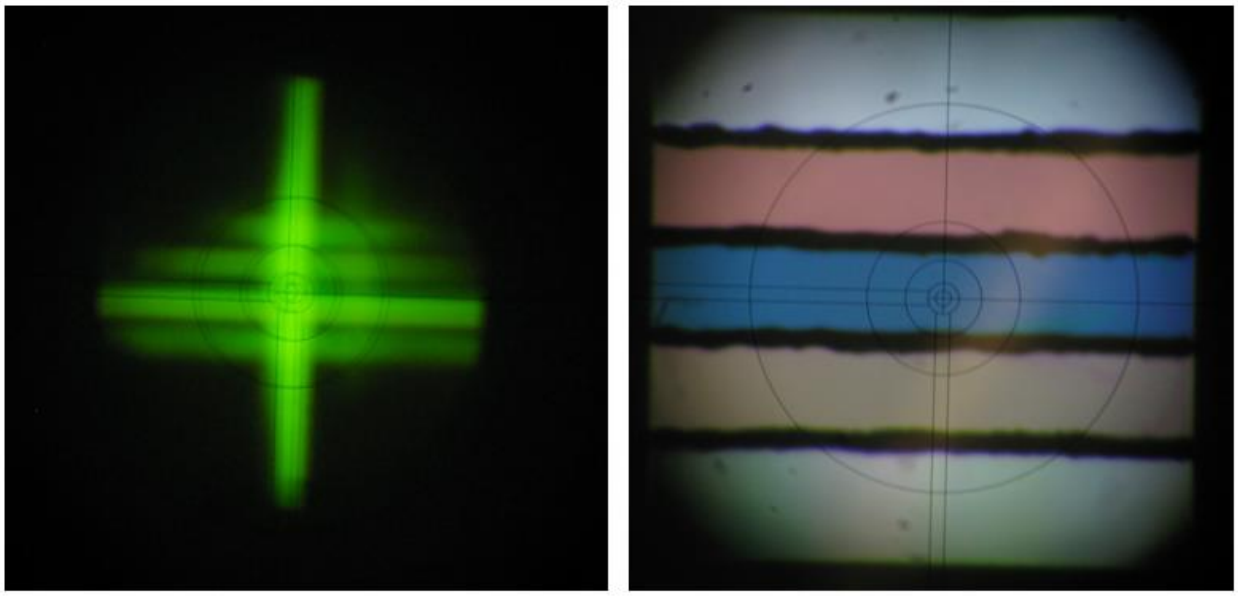

Figure 3-26. LVF through the theodolite recital at infinite (left) and finite (right) focus.

The above figure shows the results of the boresight test. We were able to use a digital camera pointed into the eyepiece of the theodolite to take photos of the theodolite return at infinite focus (on the left) as well a look at the filter itself with finite focus (on the right). The technique proved to work very well as proven by the image on the left. The azimuth was spot on in the middle of the crosshair. There were multiple returns in elevation because the filter had five different strip bonded together to create the LVF resulting in a gradient along the elevation circle with its own individual point vector.

3.10 SYSTEM MEASUREMENT

During the alignment and integration phase of OVIRS, the wavefront error --- as measured by the interferometer --- was the metric for verifying the alignment as each element was integrated into the system. The wavefront error was no longer the metric for metrology once the detector assembly became integrated into the system, because the LVF element prevented interferometry. Therefore, the theodolite measurement became the primary metric for determining system-level changes after LVF and detector installation. The system-level tests for the instrument in order were: (1) pre-post vibration test (i.e., "settling vibration test," with no LFV and detector), (2) detector installation, (3) pre-post cryogenic test 1, (4) pre-post vibration tests at ambient, (5) and, lastly, pre-post cryogenic test 2**.**

3.10.1 Pre-Detector Installation

After the installation of the primary and secondary mirror as well as the flight field stop, a flat mirror was placed at the end of the optical path to enable a system end-to-end wavefront test via autocollimator. At this point, the detector was not installed and, therefore, it was possible it place a flat mirror in the system to complete a double pass test with the interferometer and check the system alignment by measuring the wavefront error of the system. The test is illustrated in Figure 3-27 below.

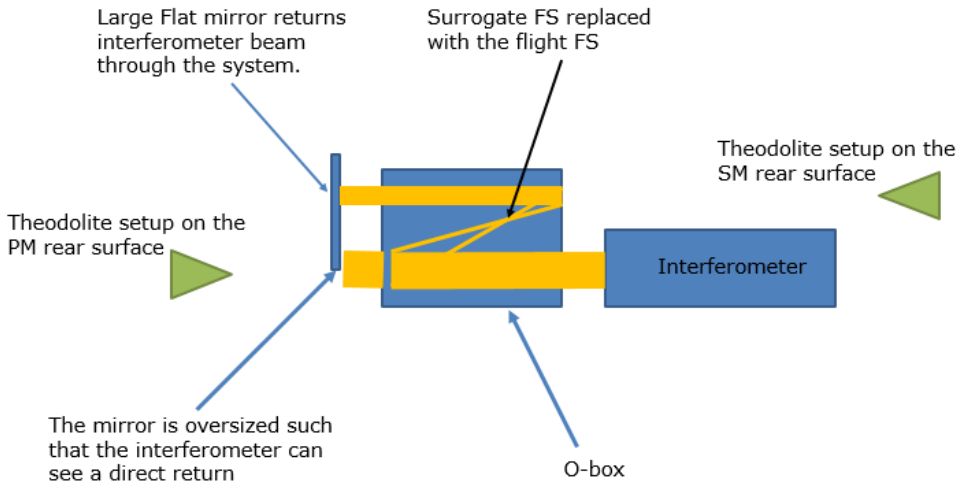

Figure 3-27. End-to-end system wavefront test schematic.

At this point during the alignment and integration flow, the first vibration test was run. This served as a "settling vibe" test. This vibration test allowed the mounted components to settle into their position within the Obox and relieve mounting stresses, reducing the risk of

component alignment change during future vibration and cryogenic exposure. The first system-level wavefront test served as the baseline for this test. The baseline pre-vibration system end-to-end wavefront error results met the requirement and can be seen in Figure 3-28.

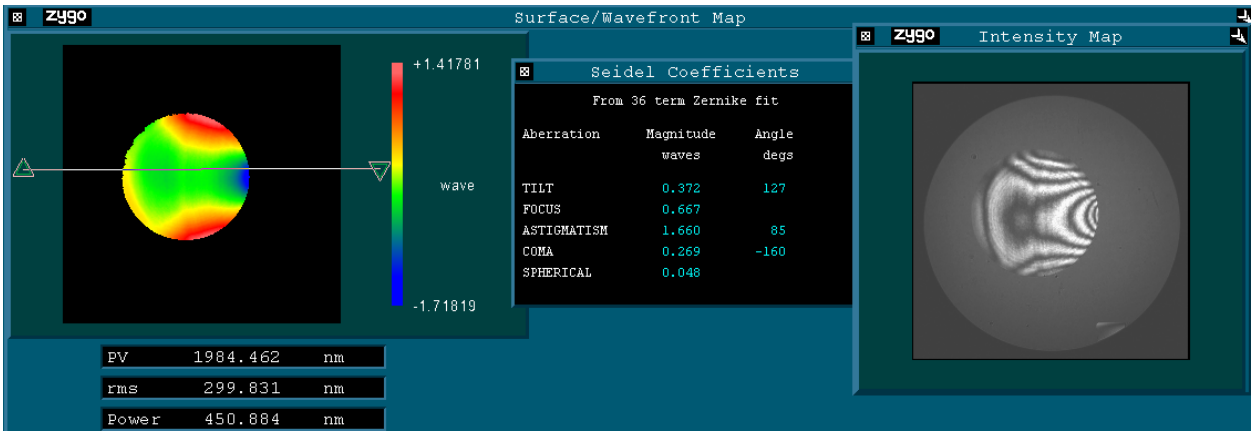

Figure 3-28. System wavefront error pre-vibration test results.

Upon completion of the settling vibration test, the instrument was then placed in front of the interferometer for the post-vibration test. The result of the test from pre- to post-vibe were within the requirement placed on allocated for RMS change. The change met the error budget allocation. The post-vibration results are shown below in Figure 3-29.

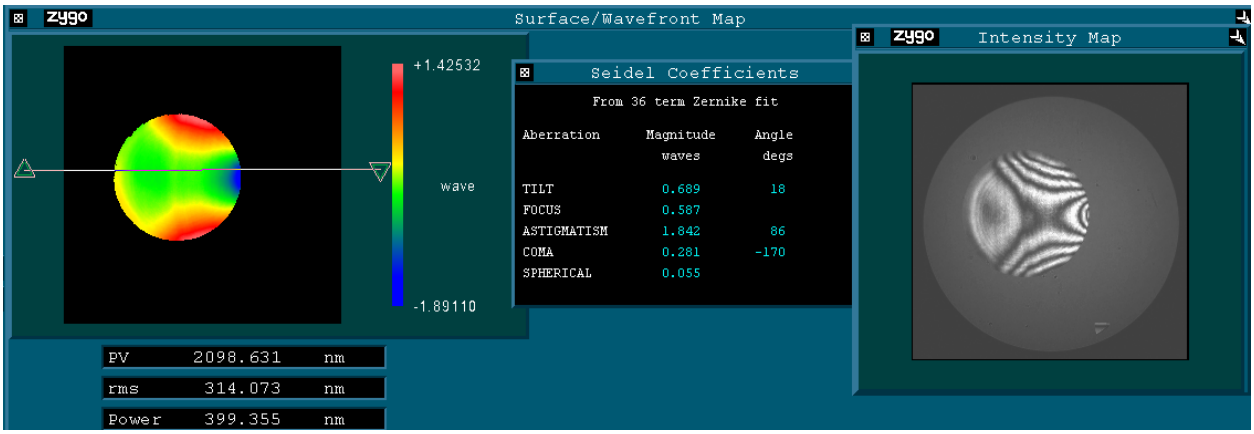

Figure 3-29. System wavefront error post-vibration test results.

Interferometry was not the only test used to evaluate the instrument's pre-and post-vibration state. Theodolites were used to measure OC1, OC2, the back surface of the primary and secondary mirror, the clocking fiducials of the primary and secondary, the autocollimating flat mirror, and the pointing of the interferometer. The laser radar was used to measure the three Obox nest targets, OB1-3. These metrology results from pre/post vibration testing are presented in the three tables below.

Table 3-2. Pre-Post Vibration Theodolite Test (OC1, OC2, Interferometer, Flat Mirror)

					Roll about X			Zenith			Pitch about Y			Yaw about Z		
vector name	*shot #*	*Mx*	*My*	*Mz*	*deg*	*min*	*sec*	*deg*	*min*	*sec*	*deg*	*min*	*sec*	*deg*	*min*	*sec*
OC1	+Y	0.00313	0.999993	0.002214	270	7	37	89	49	14	324	43	49	359	49	14
Pre-Vibe		0.00313	0.999993	0.002214	270	7	37	89	49	14	324	43	49	359	49	14
Pre-Vibe Delta					0	0	0	0	0	0	0	0	0	0	0	0
OC1	-Z	0.000153	0.002236	-1	180	7	41	89	59	28	89	59	28	356	4	56
Pre-Vibe		0.000153	0.002289	-1	180	7	52	89	59	28	89	59	28	356	10	3
Pre-Vibe Delta					0	0	11	0	0	0	0	0	0	0	5	7
Interferometer	-Z	-0.00045	-0.00067	-1	179	57	42	90	1	33	90	1	33	146	9	10
Pre-Vibe		-0.00067	-0.00016	-1	179	59	27	90	2	19	90	2	19	103	16	56
Pre-Vibe Delta					0	1	46	0	0	46	0	0	46	-42	-52	-14
OC2	-Y	-0.00148	-1	0.001401	89	55	11	90	5	6	223	22	32	179	54	54
Pre-Vibe		-0.00139	-1	0.001482	89	54	54	90	4	47	226	48	2	179	55	13
Pre-Vibe Delta					0	0	-17	0	0	-19	3	25	30	0	0	19
OC2	-Z	0.003833	-0.00143	-0.99999	179	55	5	89	46	49	89	46	49	249	33	5
Pre-Vibe		0.003712	-0.00147	-0.99999	179	54	57	89	47	14	89	47	14	248	24	41
Pre-Vibe Delta					0	0	-8	0	0	25	0	0	25	-1	-8	-24
Flat Mirror	+Z	0.000507	0.000682	1	359	57	39	89	58	15	270	1	45	323	22	46
Pre-Vibe		0.000705	0.000247	1	359	59	9	89	57	35	270	2	25	289	17	4
Pre-Vibe Delta					0	1	30	0	0	-41	0	0	41	-34	-5	-42

Table 3-3. Pre-Post Vibration Theodolite Test (OC1 and Mirrors)

					Roll about X			Zenith			Pitch about Y			Yaw about Z		
vector name	*shot #*	*Mx*	*My*	*Mz*	*deg*	*min*	*sec*	*deg*	*min*	*sec*	*deg*	*min*	*sec*	*deg*	*min*	*sec*
OC1	-x	-1	0.003131	-0.00017	266	53	47	179	49	13	179	59	25	89	49	14
Pre-Vibe		-1	0.003131	-0.00017	266	53	38	179	49	13	179	59	25	89	49	14
Pre-Vibe Delta					0	0	-9	0	0	0	0	0	0	0	0	0
OC1	-z	0.000153	0.002201	-1	180	7	34	89	59	28	89	59	28	356	1	20
Pre-Vibe		0.000153	0.002201	-1	180	7	34	89	59	28	89	59	28	356	1	20
Pre-Vibe Delta					0	0	0	0	0	0	0	0	0	0	0	0
Primary Mirror	-z	-0.00066	-0.00077	-1	179	57	21	90	2	17	90	2	17	139	10	20
Pre-Vibe		-0.00085	-0.00057	-1	179	58	3	90	2	56	90	2	56	123	38	52
Pre-Vibe Delta					0	0	41	0	0	39	0	0	39	-15	-31	-28
Primary Clocking Fiducial	-x	-1	-0.00015	0.000739	11	40	56	179	57	24	180	2	32	90	0	32
Pre-Vibe		-1	-0.00014	0.000935	8	47	1	179	56	45	180	3	13	90	0	30
Pre-Vibe Delta					-2	-53	-55	0	0	-39	0	0	40	0	0	-2
Secondary Mirror	+z	-0.00064	-0.0008	0.999999	0	2	45	90	2	11	269	57	49	141	29	29
Pre-Vibe		-0.00048	-0.0009	0.999999	0	3	6	90	1	38	269	58	22	152	12	42
Pre-Vibe Delta					0	0	21	0	0	-33	0	0	33	10	43	13
Secondary Clocking Fiduci	-x	-1	0.000291	-0.00243	186	50	14	179	51	35	179	51	39	89	58	60
Pre-Vibe		-1	0.00011	-0.0023	182	44	42	179	52	5	179	52	5	89	59	37
Pre-Vibe Delta					-4	-5	-33	0	0	30	0	0	27	0	0	37

Table 3-4. Pre-Post Vibration Laser Radar Results

	Post Vibe			Pre-vibe			Pre-Post		
Post-vibe	X	Y	Z	X	Y	Z	X	Y	Z
OB1	-181.610	-0.020	-0.043	-181.610	-0.014	-0.047	0.000	0.006	-0.004
OB2	-181.610	-145.902	443.227	-181.610	-145.899	443.238	0.000	0.002	0.011
OB3	-181.610	145.960	443.326	-181.610	145.952	443.319	0.000	-0.008	-0.006

The pre/post-vibration changes in system alignment for the objects and degrees of freedom that were measureable (at this level of assembly) met requirements. For comparison to requirements, measurement error and these changes were combined. While this approach is conservative, it demonstrates with high likelihood that the system is stable to required levels. The mirrors were measured in tip/tilt and clocking (i.e., all three rotations). Measurement of fiducials for translations was not possible at this level of assembly, but it was assumed that stability in rotations is a likely indicator of stability in translations as well. Obox nest target stability indicates that bench did not significantly deform during the vibration test, supporting this assumption. Coupled with the system wavefront error measurement, this supports the position that the mirrors are stable with respect to each other and the bench coordinate system.

3.10.2 Post Detector Installation

After the installation of the LVF and detector subsystem, it was no longer possible to complete an end-to-end wavefront error test, because, even though the LVF was able to provide an interferometric return, the five different substrates that composed the LFV produced their own, unique fringe pattern over their sub-aperture of the pupil. The instrument Obox covers were also added to the system, blocking line of sight to the internal components and their fiducials. The only available targets for metrology were OC1, OC2, the Obox nest targets, and the interferometer pointing as an external reference. The boresight of the instrument in reference to OC1 became the metric against which the internal alignment was trended from this point forward.

Furthermore, rough boresight trending was performed pre/post-instrument-level vibration and cryogenic testing using theodolite measurements both at infinite conjugate and finite conjugate in the same manner as the tests described in Section 3.9. While low fidelity, these served as a cross check and results were consistent with those from the lower uncertainty metrology pre/post-settling vibe. In this manner, it was determined that the system was stable pre/post-vibration and cryogenic exposure after the detector was installed (i.e., at the full

instrument-level). A photograph of the instrument on its vibration plate before the vibe test is shown in Figure 3-30.

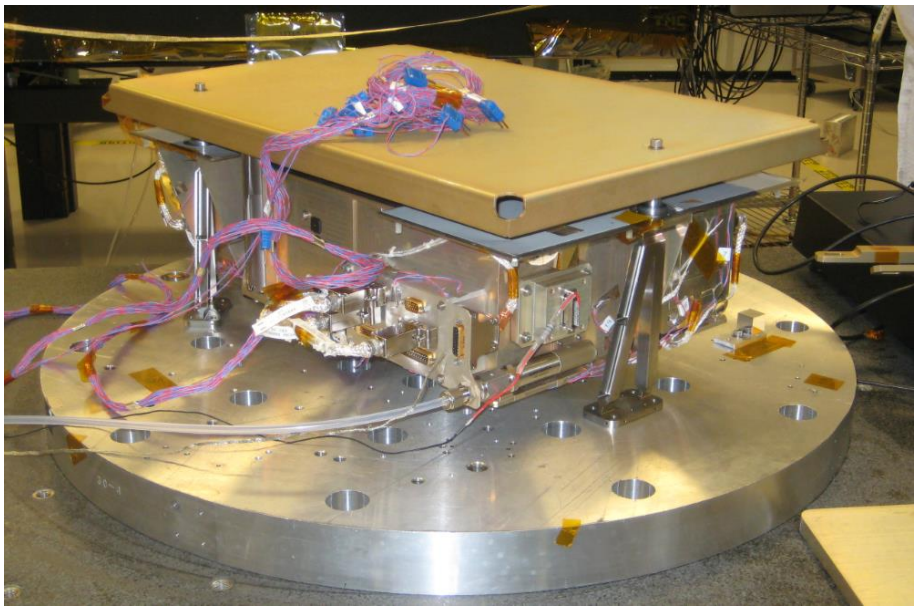

Figure 3-30. OVIRS on the vibration test plate.

Images and metrology data showing the trending of the ambient instrument boresight testing through the system level testing are shown in the figures below. The data from OC1 and the interferometer return off from the LVF are shown in Figure 3-31. The data from OC1 and the theodolite return from it at an infinite conjugate are shown in Figure 3-32.

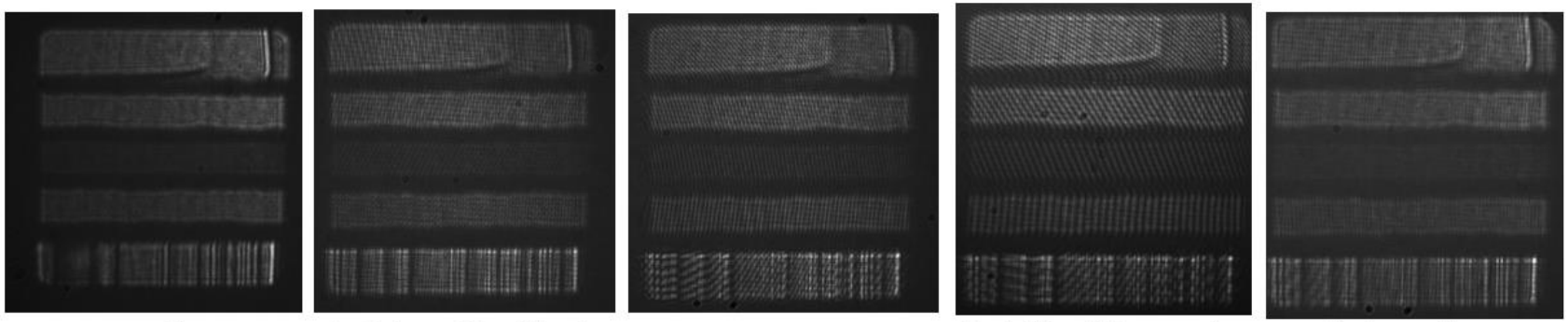

Interferometer Test/Instrument Pointing		CS: OVIRS via Obox nests			roll			zenith			pitch			yaw		
vector name	*shot #*	*Mx*	*My*	*Mz*	*deg*	*min*	*sec*	*deg*	*min*	*sec*	*deg*	*min*	*sec*	*deg*	*min*	*sec*
OC1 +Y	Pre-Settling Vibe-No Det	0.003240444	0.999992579	0.002083637	270	7	10	89	48	52	327	15	31	359	48	52
	Post-Settling Vibe-No Det	0.003130107	0.999992651	0.00221375	270	7	37	89	49	14	324	43	49	359	49	14
	*Pre-Cryo 1	0.003130106	0.999992639	0.002219156	270	7	38	89	49	14	324	39	52	359	49	14
	*Post-Cryo 1/Pre-Vibe 1	0.003243822	0.999992978	0.001876965	270	6	27	89	48	51	329	56	47	359	48	51
	Post-Vibe 1/Pre-Vibe 2	0.003243819	0.999992967	0.001882746	270	6	28	89	48	51	329	52	7	359	48	51
	*Post-Vibe 2/Pre-Cryo 2	0.002919327	0.999993757	0.001990691	270	6	51	89	49	58	325	42	35	359	49	58
	*Post-Cryo 2	0.003294955	0.999992483	0.002043906	270	7	2	89	48	40	328	11	17	359	48	40
	95% Uncertainty (3σ)				0	1	26	0	1	32	7	7	23	0	1	32
OC1 -Z	Pre-Settling Vibe-No Det	0.000198664	0.0021528	-0.999997663	180	7	24	89	59	19	89	59	19	354	43	39
	Post-Settling Vibe-No Det	0.000153154	0.002236298	-0.999997488	180	7	41	89	59	28	89	59	28	356	4	56
	*Pre-Cryo 1	0.000153082	0.002213282	-0.999997539	180	7	37	89	59	28	89	59	28	356	2	36
	*Post-Cryo 1/Pre-Vibe 1	0.000530531	0.001881034	-0.99999809	180	6	28	89	58	11	89	58	11	344	14	58
	Post-Vibe 1/Pre-Vibe 2	0.000530445	0.001854733	-0.999998139	180	6	23	89	58	11	89	58	11	344	2	23
	*Post-Vibe 2/Pre-Cryo 2	0.000404336	0.001975494	-0.999997967	180	6	47	89	58	37	89	58	37	348	25	58
	*Post-Cryo 2	0.000452069	0.002034716	-0.999997828	180	6	60	89	58	27	89	58	27	347	28	25
	95% Uncertainty (3σ)				0	1	28	0	1	35	0	1	35	14	25	14
Interferometer -Z	Pre-Settling Vibe-No Det	-0.000680379	-0.000288551	-0.999999727	179	59	0	90	2	20	90	2	20	112	58	55
	Post-Settling Vibe-No Det	-0.000449796	-0.000670697	-0.999999674	179	57	42	90	1	33	90	1	33	146	9	10
	*Pre-Cryo 1	-0.000766329	0.000164026	-0.999999693	180	0	34	90	2	38	90	2	38	77	55	7
	*Post-Cryo 1/Pre-Vibe 1	-0.000826131	-5.13654E-05	-0.999999657	179	59	49	90	2	50	90	2	50	93	33	28
	Post-Vibe 1/Pre-Vibe 2	-0.00140465	0.000448749	-0.999998913	180	1	33	90	4	50	90	4	50	72	16	58
	*Post-Vibe 2/Pre-Cryo 2	-0.000925707	-3.84818E-05	-0.999999571	179	59	52	90	3	11	90	3	11	92	22	50
	*Post-Cryo 2	-0.001001452	0.000156936	-0.999999486	180	0	32	90	3	27	90	3	27	81	5	37
	95% Uncertainty (3σ)				0	2	4	0	2	34	0	2	34	27	24	24

Figure 3-31. Trending data from the interferometer and theodolite alignment test (infinite conjugate).

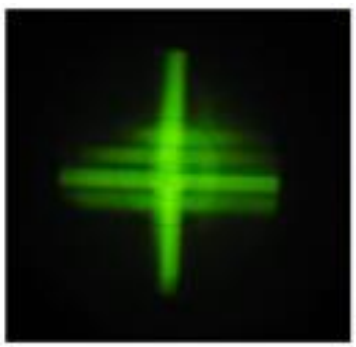

Pre-Cryo 1

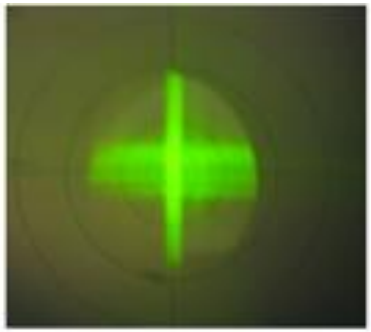

Post-Cryo 1/Pre-Vibe 1

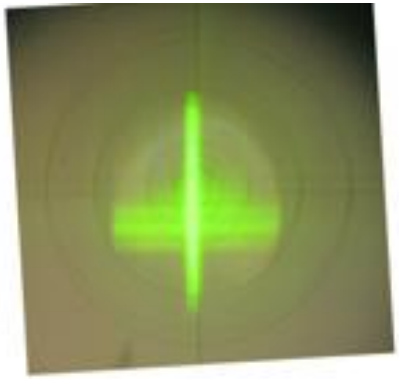

Post-Vibe 1/Pre-Vibe 2

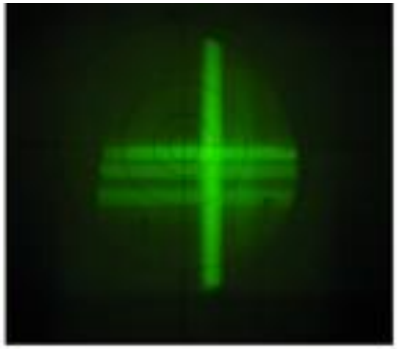

Post-Vibe 2/Pre-Cryo 2

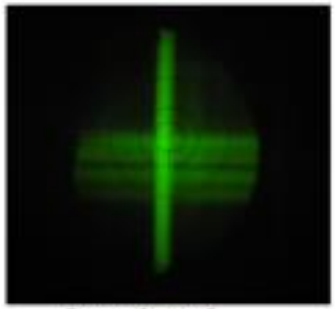

Post-Cryo 2

Ring 1=10 asecs from center
Ring 2=
Ring 3=
Ring 4=

This table shows how well each test was aligned to the nominal boresight

Interferometer Test/Instrument Pointing					roll			zenith			pitch			yaw		
vector name	shot #	Mx	My	Mz	deg	min	sec	deg	min	sec	deg	min	sec	deg	min	sec
Shot Line	Pre-Cryo 1	0.001035	0.000353	0.999999	359	58	47	89	56	26	270	3	34	288	50	19
	Post-Cryo 1/Pre-Vibe 1	0.001009	0.000342	0.999999	359	58	49	89	56	32	270	3	28	288	43	27
	Post-Vibe 1	0.001063	0.00028	0.999999	359	59	2	89	56	21	270	3	39	284	44	13
	95% Uncertainty				0	0	20	0	0	14	0	0	14			

Figure 3-32. Trending data from the interferometer and theodolite alignment test (finite conjugate).

In summary, the OVIRS instrument was shown to meet its wavefront error and stability requirements during ground integration and test. Optical cube OC1 was calibrated relative to the boresight pointing direction of the instrument (i.e., OC1 served as an angular reference for the chief ray at the center field point), useful for instrument-to-spacecraft alignment. The OVIRS instrument met its ambient alignment and performance requirements, setting the stage for a successful cryogenic performance test and setting the expectation for successful on-orbit function and performance. After the work described here, OVIRS was successfully delivered to the project for integration with the spacecraft (Figure 3-33).

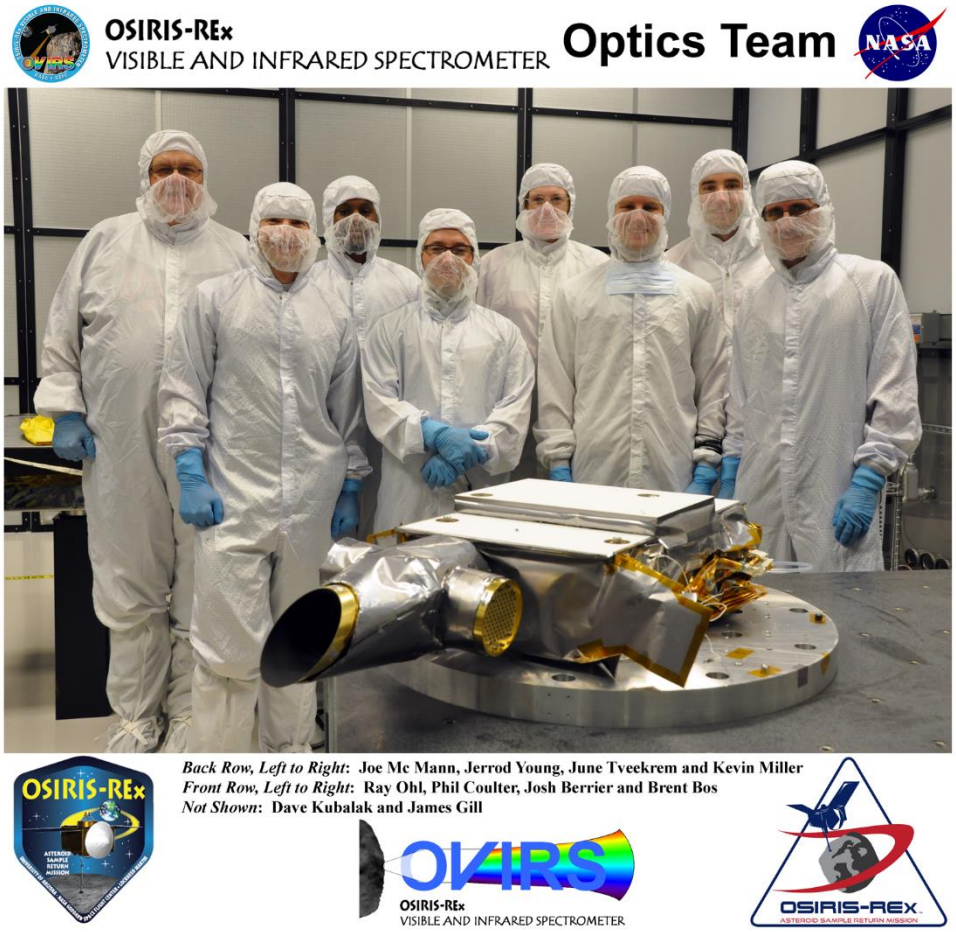

Figure 3-33. Image showing completed OVIRS instrument and team.

4.0 REFERENCES

1. https://istd.gsfc.nasa.gov/551/
2. Coulter, Phillip, et al. "A toolbox of metrology-based techniques for optical system alignment." *SPIE Optical Engineering+ Applications*. International Society for Optics and Photonics, 2016.
3. A. Slotwinski and P. Blanckaert, "Frequency Modulated Coherent Laser Radar Technology," Proceedings of the OPTIMESS2007 Workshop, Leuven, Belgium, May 28—30, 2007.
4. J. H. Burge, P. Su, C. Zhao and T. Zobrist, "Use of a Commercial Laser Track for Optical Alignment", Proc. SPIE 6676, 66760E, 66760E-12 (2007).
5. B. B. Gallagher, *Optical Shop Applications for Laser Tracker Metrology Systems*, (M.S. Thesis, College of Optical Sciences, University of Arizona, 2003).
6. T. Zobrist, "Application of Laser Tracker Technology for Measuring Optical Surfaces," Ph.D. dissertation (University of Arizona, 2009).
7. S. E. Hetherington, D. Osgood, J. McMann, V. Roberts, J. E. Gill, K. McLean, "Optical Alignment of the Global Precipitation Measurements (GPM) Star Trackers", *Proc. Optical System Alignment Tolerancing and Verification VII 2013*, vol. 8844, no. 884406.
8. K. Redman, "Spacecraft optical alignment measurements and analysis process," Unpublished.
9. W. L. Eichhorn, "Optical Alignment Measurements at Goddard Space Flight Center", Applied Optics, 21, 3891-3895 (1982).
10. Whitman, T., "OAFDAP manual (version 1.1)," Unpublished.
11. C. Aviado, J. Gill, K. Redman and R. Ohl, "Methods for Correlating Autocollimation of Theodolites and Coordinate Metrologu in Spacecraft Systems", Proc. SPIE 6273, 62733H-8 (2006)
12. Micro-Vu Corporation, Windsor, California, https://www.microvu.com/products/sol.html
13. S. Sandwith and R. Predmore, "Real-time 5-Micron Uncertainty with Laser Tracking Interferometer Systems using Weighted Trilateration," Proc. SPIE.
14. Spatial Analyzer Users Manual, New River Kinematics, Williamsburg, v. 1.21.2008, page 150.
15. New River Kinematics, Inc., Williamsburg, Va., www.kinematics.com
16. Leica Geosystems AG, Heerbrugg, Switzerland, metrology.leica-geosystems.com
17. https://www.nasa.gov/osiris-rex
18. D.C. Reuter, et al. "The OSIRIS-REx visible and infrared spectrometer (OVIRS): spectral maps of the asteroid Bennu" Space Sci. Rev. Vol. 212 (2017)

19. D. C. Reuter and A. A. Simon-Miller, The OVIRS Visible IR Spectrometer on the OSIRIS-REx Mission., 'NASA/GSFC, Code 693, Greenbelt, MD 20771, 2 NASA/GSFC, Code 690, Greenbelt, MD 20771.

20. [1] Simon-Miller, A. A.; Reuter, D. C. "OSIRIS-REx OVIRS: A Scalable Visible to Near-IR Spectrometer for Planetary Study," 44th Lunar and Planetary Science Conference, held March 18-22, 2013 in The Woodlands, Texas. LPI Contribution No. 1719, p.1100.

21. R. Ohl, OVIRS Instrument Alignment Plan, PLA-OSIRIS-REX-OVIRS-PLAN-0048, Dec 2013, Unpublished

22. Corning Specialty Materials, Keen, New Hampshire

23. Zygo Corp. Verifire ca. 2003, https://www.zygo.com/?/met/interferometers/interferometer.htm, Zygo Corp., Middlefield, Connecticut

24. J. MacKenty, R. Green, M. Greenhouse, and R. Ohl, Design and performance of a MEMS-based infrared multi-object spectrometer, *Proc. SPIE* 5492, 1105, 2004)